Atmos. Chem. Phys., 24, 4129–4155, 2024
https://doi.org/10.5194/acp-24-4129-2024

Atmospheric Chemistry and Physics
Open Access
EGU

Measurement report: Bio-physicochemistry of tropical clouds at Maïdo (Réunion, Indian Ocean): overview of results from the BIO-MAÏDO campaign

Maud Leriche[1,2], Pierre Tulet[3], Laurent Deguillaume[1,4], Frédéric Burnet[5], Aurélie Colomb[1], Agnès Borbon[1], Corinne Jambert[3], Valentin Duflot[6], Stéphan Houdier[7], Jean-Luc Jaffrezo[7], Mickaël Vaïtilingom[8], Pamela Dominutti[1,7], Manon Rocco[1,a], Camille Mouchel-Vallon[3], Samira El Gdachi[3,6], Maxence Brissy[1,9], Maroua Fathalli[5], Nicolas Maury[5], Bert Verreyken[10,11,6,b,c], Crist Amelynck[10,11], Niels Schoon[10], Valérie Gros[12], Jean-Marc Pichon[4], Mickael Ribeiro[1], Eric Pique[3], Emmanuel Leclerc[3], Thierry Bourrianne[5], Axel Roy[5], Eric Moulin[5], Joël Barrie[5], Jean-Marc Metzger[13], Guillaume Péris[14], Christian Guadagno[14], Chatrapatty Bhugwant[14], Jean-Mathieu Tibere[14], Arnaud Tournigand[14], Evelyn Freney[1], Karine Sellegri[1], Anne-Marie Delort[9], Pierre Amato[9], Muriel Joly[9], Jean-Luc Baray[1,4], Pascal Renard[1], Angelica Bianco[1], Anne Réchou[6], and Guillaume Payen[13]

[1]Laboratoire de Météorologie Physique (LaMP), UMR 6016, CNRS, Université Clermont Auvergne, Aubière, 63178, France
[2]Centre pour l'étude et la simulation du climat à l'échelle régionale, Département des sciences de la terre et de l'atmosphère (ESCER), Université du Québec à Montréal, Montréal, H2X 3Y7, Canada
[3]Laboratoire d'Aérologie (LAERO), UMR 5560, CNRS, Université Paul Sabatier, IRD, Toulouse, 31400, France
[4]Observatoire de Physique du Globe de Clermont-Ferrand (OPGC), UAR 833, CNRS, Université Clermont Auvergne, Aubière, 63178, France
[5]Centre National de Recherches Météorologiques (CNRM), UMR 3589, CNRS, Université de Toulouse, Météo-France, Toulouse, 31057, France
[6]Laboratoire de l'Atmosphère et des Cyclones (LACy), UMR 8105, CNRS, Université de la Réunion, Météo-France, Saint-Denis de la Réunion, 97744, France
[7]Institut des Géosciences de l'Environnement (IGE), UMR 5001, CNRS, IRD, Université Grenoble Alpes, Grenoble, 38000, France
[8]Laboratoire de Recherche en Géosciences et Énergies (LaRGE), EA 4539, Université des Antilles, Pointre-à-Pitre, 97110, France
[9]Institut de Chimie de Clermont-Ferrand (ICCF), UMR 6296, CNRS, Université Clermont Auvergne, Aubière, 63178, France
[10]Royal Belgian Institute for Space Aeronomy (BIRA-IASB), Brussels, 1180, Belgium
[11]Departement of Chemistry, Ghent University, Ghent, 9000, Belgium
[12]Laboratoire des Sciences du Climat et de l'Environnement (LSCE), UMR 8212, CNRS, CEA, Université Versailles Saint Quentin, Gif-sur-Yvette, 91198, France
[13]Observatoire des Sciences de l'Univers de La Réunion (OSUR), UAR 3365, Saint-Denis de la Réunion, 97744, France
[14]ATMO-Réunion, Sainte-Marie, 97438, France
[a]now at: Laboratoire de Chimie de l'Environnement (LCE), UMR 7376, CNRS, Aix-Marseille Université, Marseille, 13331, France
[b]now at: The Royal Belgian Institute for Space Aeronomy (BIRA-IASB), Brussels, 1180, Belgium
[c]now at: Gembloux Agro-Biotech, University of Liège, Gembloux, 5030, Belgium

Correspondence: Maud Leriche (m.leriche@opgc.fr) and Pierre Tulet (pierre.tulet@aero.obs-mip.fr)

Published by Copernicus Publications on behalf of the European Geosciences Union.

Received: 22 June 2023 – Discussion started: 1 August 2023
Revised: 22 December 2023 – Accepted: 12 February 2024 – Published: 8 April 2024

Abstract. The BIO-MAÏDO (Bio-physicochemistry of tropical clouds at Maïdo: processes and impacts on secondary organic aerosols formation) campaign was conducted from 13 March to 4 April 2019 on the tropical island of Réunion. The main objective of the project was to improve understanding of cloud impacts on the formation of secondary organic aerosols (SOA) from biogenic volatile organic compound (BVOC) precursors in a tropical environment. Instruments were deployed at five sites: a receptor site, Maïdo Observatory (MO) at 2165 m a.s.l. and four sites along the slope of the Maïdo mountain. Observations include measurements of volatile organic compounds (VOCs) and characterization of the physical, chemical and biological (bacterial diversity and culture-based approaches) properties of aerosols and cloud water. Turbulent parameters of the boundary layer, radiative fluxes and emissions fluxes of BVOCs from the surrounding vegetation were measured to help interpret observed chemical concentrations in the different phases. Dynamical analyses showed two preferred trajectory routes for air masses arriving at MO during the daytime. Both trajectories correspond to return branches of the trade winds associated with upslope thermal breezes, where air masses likely encountered cloud processing. The highest mixing ratios of oxygenated VOCs (OVOCs) were measured above the site located in the endemic forest and the highest contribution of OVOCs to total VOCs at MO. Chemical compositions of particles during daytime showed higher concentrations of oxalic acid, a tracer of cloud processing and photochemical aging, and a more oxidized organic aerosol at MO than at other sites. Approximately 20 % of the dissolved organic compounds were analyzed. Additional analyses by ultra-high-resolution mass spectrometry will explore the complexity of the missing cloud organic matter.

1 Introduction

Aerosols are essential components in the atmosphere as a result of their role in the radiative budget of the earth, including their indirect impact by acting as cloud condensation nuclei (CCN) and ice nuclei (IN) in the formation of cloud droplets and ice crystals. Their impact on climate is still uncertain (Boucher et al., 2013). Aerosols are also a major contributor to air pollution, and their health effects have been demonstrated (World Health Organization, 2021). However, there are still major uncertainties in the formation and transformation of atmospheric aerosols. These uncertainties need to be removed to understand the impacts of these particles on air quality, health and climate change. Atmospheric aerosols have a complex chemical composition, and the organic fraction, which contributes significantly to the total mass of fine particles (Jimenez et al., 2009), is still the least characterized to date. Three-dimensional atmospheric chemistry models are globally unable to reproduce the observed amount, oxidation level and spatial distribution of organic aerosols (Heald et al., 2011; Jathar et al., 2016; Pai et al., 2020). Among this organic fraction, a major part of the mass is of secondary origin (Zhang et al., 2007). The main precursors of secondary organic aerosols (SOA) are natural compounds (isoprene and terpenes) and aromatics of anthropogenic origin. Even if the chemical reactivity in the gaseous phase of these volatile organic compounds (VOCs) is relatively well known, the nature and potential of SOA formation of their oxidation products are still uncertain. Biogenic VOCs (BVOCs) from terrestrial vegetation are particularly important since they dominate the global emission of non-methane hydrocarbons in the atmosphere (Guenther et al., 2012). The oxidation of BVOCs in the atmosphere forms less volatile oxidized chemical species, which participate in SOA formation through various complex processes (Shrivastava et al., 2017). These oxidized products are soluble in water, where they are photooxidized (Ervens et al., 2011). The chemical reactivity in the aqueous phase is different than in the gas phase and can lead to the formation of low-volatility compounds (Carlton et al., 2007; Yao Liu et al., 2009), including oligomers (Renard et al., 2015). It is now well established that the aqueous-phase oxidation contribution to the SOA formation is significant (McNeil, 2015; Su et al., 2020, under polluted conditions) but still misunderstood in terms of processes and badly represented in 3D models (Ervens, 2015). The main contributors to SOA formation from cloud chemistry are known to be low-volatility organic acids coming mainly from the photooxidation of glyoxal and methylglyoxal (Ervens et al., 2011). Recently, Tsui et al. (2019) showed that isoprene epoxydiols (IEPOX) could be a significant contributor to SOA formation from cloud chemistry. The presence of bacteria in cloud water also has a potential impact on cloud chemical composition (Vaïtilingom et al., 2013; Khaled et al., 2021). A recent study on the global scale estimates that microbial processes might lead to a loss of water-soluble organic content in cloud droplets on the same order of magnitude as the loss from chemical processes (Ervens and Amato, 2020). However, this estimation is very uncertain, and, to the best of our knowledge, no study has assessed the effect of microbial processes in cloud droplets on SOA formation.

Humid tropical atmospheres, which are characterized by high biogenic emissions and a high occurrence of fogs and clouds, is particularly favorable to SOA formation through biogenic precursors via cloud multiphase chemistry. Réunion is a small tropical island in the Indian Ocean to the east of Madagascar. Anthropogenic sources are limited on the island and are mainly in the coastline area, as the island is far from the impact of large anthropogenic emission sources (Duflot et al., 2019). Réunion is a volcanic island with an abrupt topography and a high mountainous area (Piton des Neiges, 3070 m) and presents 100 000 ha of native ecosystems (Duflot et al., 2019). Lesouëf et al. (2011, 2013) described the complex atmospheric dynamic on the island, which is, at the large scale, affected by easterly and southeasterly trade winds near the ground and westerlies in the free troposphere. Due to the strengthening of the large-scale subtropical subsidence at night, air masses at high altitude are disconnected from local and regional anthropogenic sources during the night and early morning.

The Maïdo atmospheric observatory (altitude 2165 m) (Baray et al., 2013), close to the Piton Maïdo (2190 m), is in the northwestern part of the island and offers a unique opportunity to study SOA formation processes in the humid tropical atmosphere. The slope of the Maïdo, west of the observatory, is covered with tropical forests characterized by the endemic tree species *Acacia heterophylla* (Fabaceae), plantations of the coniferous species *Cryptomeria japonica* (Taxodiacae) and the *Acacia heterophylla* forest, locally called "Tamarinaie" (Duflot et al., 2019). A first campaign devoted to cloud–aerosol interaction (Duflot et al., 2019) in March–April 2015 showed the potential of the observatory to study the formation of SOA influenced by clouds with the diurnal formation of clouds on the slope below the observatory over Tamarinaie (which emits isoprene and terpenes) and their dissipation at the level of the observatory. Measurements performed during this campaign showed high levels of formaldehyde, a product of isoprene oxidation, and the presence of viable bacteria in cloud water.

The BIO-MAÏDO (Bio-physicochemistry of tropical clouds at Maïdo (Réunion): processes and impacts on secondary organic aerosols formation) project was designed in this context with three main objectives: (i) to understand which are the main formation pathways of SOA in a humid tropical atmosphere (gaseous phase versus aqueous phase), (ii) to improve multiphase processes leading to SOA formation in a 3D model, and (iii) to examine whether the presence of bacteria in the aqueous phase could contribute to SOA formation. The strategy of BIO-MAÏDO is based on an intensive field campaign using the Maïdo Observatory facilities, in synergy with modeling studies using two Lagrangian particle dispersion models, FLEXPART-AROME (Verreyken et al., 2019) and Meso-CAT (Rocco et al., 2022), a 0D cloud chemistry model (CLEPS, Mouchel-Vallon et al., 2017; Rose et al., 2018) and a 3D model coupling meteorology and chemistry and including a cloud chemistry module (Meso-NH, Lac et al., 2018; http://mesonh.aero.obs-mip.fr/, last access: 20 June 2023).

The aim of the present paper is to present an overview of the results obtained from the campaign, including new analyses compared to previous studies (Rocco et al., 2022; Dominutti et al., 2022a, b). First, the general strategy of the campaign and the description of the five sampling sites are provided. Then, the main results obtained from the measurements are summarized. The main meteorological circulations at the synoptic and local scales are analyzed, and the dynamical context of a typical cloudy day during the campaign is detailed. Observations of VOCs during the campaign are summarized and compared to other VOC measurements on Réunion. For aerosol observations, after summarizing the main results obtained previously, we discuss the comparison between chemical composition from filters sampled at the lowest site and at Maïdo Observatory. Cloud chemistry analyses are summarized, and ongoing work is presented. For biological measurements, we briefly present the diversity of culturable bacteria from cloud samples and the bacteria diversity profiling from aerosol filters. Finally, we discuss from a general perspective the results obtained from the campaign.

2 Strategy of the campaign and site description

2.1 Strategy

In the general context of the three main objectives of the BIO-MÄIDO project presented above, the field campaign aims to (1) characterize the chemical and biological composition of air and cloud samples and identify the main sources of gases and aerosols, (2) characterize the dynamics and evolution of the boundary layer and the macrophysical and microphysical properties of clouds, and (3) determine case studies for modeling work with CLEPS and Meso-NH.

The campaign took place from 13 March to 4 April 2019. This period was chosen to include frequent periods of formation of low-level clouds and of convective precipitating clouds along the slopes of the Maïdo (Duflot et al., 2019), a high UV index (12) and high temperatures (end of the southern summer). Moreover, the campaign took place during the 2-year observation period of the OCTAVE project (Oxygenated Compounds in the Tropical Atmosphere: Variability and Exchanges, https://octave.aeronomie.be/, last access: 20 June 2023), during which complementary instrumentation was deployed at Maïdo Observatory to characterize oxygenated volatile organic compound (OVOC) mixing ratios. The main objective of OCTAVE is to improve the climatology of the global budget of OVOCs and their role in tropical regions (Rocco et al., 2020; Simu et al., 2021; Verreyken et al., 2021).

The field campaign included five sampling sites (Fig. 1). Except for Maïdo Observatory, these sites are all located along the northwestern slope to the Maïdo site, identified as one of the two main paths for dominant winds (Duflot et

al., 2019). At mid-morning almost every day, clouds form on the slope of the Maïdo and in general evaporate at the altitude of the observatory (Duflot et al., 2019). The locations of the sampling sites should allow observation of the air mass processing by clouds along the slope in a Lagrangian trajectory approach where Maïdo Observatory is the receptor site.

An innovative instrumentation was deployed, including, e.g., three proton-transfer-reaction mass spectrometers (PTR-MSs) for online analysis of VOCs, one of which was operated at high frequency and coupled to an ultrasonic anemometer allowing measurements of BVOC fluxes; a tethered balloon to capture microphysical characteristics of clouds; an aerosol chemical speciation monitor (ACSM), which provides online measurements of the non-refractory submicron chemical composition (NR-PM_1); a new generation of a cloud droplet impactor to accumulate cloud water and allow biological (bacteria diversity and number concentration, adenosine triphosphate (ATP) quantification) and detailed chemical analyses further in the lab. For instance, dissolved organic compounds have been intensively investigated in cloud water to characterize their atmospheric sources, to evaluate the chemical and biological processes occurring in the air during the transport of the organic matter, and to assess their partitioning among the gas and aqueous phases.

During the whole campaign, FLEXPART (Pisso et al., 2019) coupled with the AROME operational forecasts at 2.5 km horizontal resolution (Verreyken et al., 2019) was used to analyze the regional origin (marine boundary layer, free troposphere) of the air masses observed in the Maïdo area. This information has been supplemented by back-trajectories computed with Meso-CAT (Rocco et al., 2022) resulting from the coupling between high-resolution Meso-NH simulations and the Lagrangian tool CAT (Computing Advection-interpolation of atmospheric parameters and Trajectory tool; Baray et al., 2020). These back-trajectories allowed assessment of the local contribution of a biogenic, anthropogenic and marine source area in the chemical composition of air masses sampled at the sampling sites and determination of which days present a dynamical connection between the sites.

2.2 Petite France (PF-1): a rural site under urban influence

Petite France (965 m a.s.l.; 21°02′33.3″ S, 55°19′32″ E) is a neighborhood of the municipality of Saint-Paul. The land cover around PF-1 mainly comprises residential areas, grassland, and sugarcane plantations. Some of the instruments are deployed inside the monitoring truck of Atmo-Réunion (https://atmo-reunion.net/, last access: 20 June 2023), the association in charge of the air quality monitoring on the island. Instrumentation deployed at PF-1 aims to characterize the chemical composition of the air, including gases and PM_{10}. The instrumentation on board the truck included analyzers for ozone, carbon monoxide, nitrogen oxides, sulfur dioxide, a particle counter for $PM_{2.5}$ and a PTR-QMS for online VOC characterization. The chemical and biological composition of PM_{10} was analyzed from pure quartz fiber filters sampled twice a day during night and day with a high-volume sampler. Various chemical analyses of filters were performed in the lab to quantify the major chemical constituents and specific chemical tracers. The carbonaceous fraction of particles (elemental carbon EC and organic carbon OC) was analyzed with a Sunset Lab analyzer (using the EUSAAR2 thermo-optical protocol, Cavalli et al., 2010). The major ion components were measured by ion chromatography using an ICS300 chromatograph (dual-channel, Thermo Fisher) following the standard protocol described in Jaffrezo et al. (2005). Anhydro sugars and saccharides were analyzed with high-performance liquid chromatography with pulsed amperometric detection (HPLC-PAD, using an ICS 5000+ chromatograph, Samaké et al., 2019). The analysis of organic acids was conducted using a HPLC-MS (GP40 Dionex) with negative-mode electrospray ionization (Borlaza et al., 2021). The diversity of bacteria in PM_{10} samples was investigated by high-throughput sequencing (Illumina) of meta-barcoded ribosomal gene amplicons from whole genomic DNA extracted using the commercial DNeasy PowerWater kit (Qiagen). Polymerase chain reaction (PCR) amplification was performed using the primers 515F and 806R, as recommended by the Earth Microbiome Project (Caporaso et al., 2012). The sequence data obtained from Illumina MiSeq (2×250 bp) were analyzed through the FROGS pipeline (Escudié et al., 2018) using Silva 132 as the reference database (Quast et al., 2013), as in Péguilhan et al. (2021). In addition, a ceilometer was deployed to characterize the boundary layer evolution and the cloud cycle. Table 1 summarizes the instruments deployed at PF-1 and the associated measured parameters.

2.3 Domaine des Orchidées Sauvages (DOS-2): a strategic site to observe the cloud cycle

DOS-2 (1465 m a.s.l.; 21°03′07″ S, 55°21′11″ E) is a large private property where the tethered balloon was operated. Moreover, several sets of devices were also deployed there: a meteorological station, complementary probes monitoring the size spectrum of particles, a present weather visibility sensor associated with a droplet size spectrometer to characterize the microphysical properties of clouds, as well as a ceilometer and the MARLEY (Mobile AeRosol Raman Lidar for troposphEre surveY) lidar to characterize the boundary layer evolution, the cloud cycle and the vertical profile of aerosols. The land cover around DOS-2 is composed mainly of a mix of grassland and forests.

The tethered balloon was equipped with an ultrasonic anemometer and a temperature probe at high frequency to estimate the heat and momentum fluxes and the turbulent kinetic energy by eddy covariance. At the beginning of the

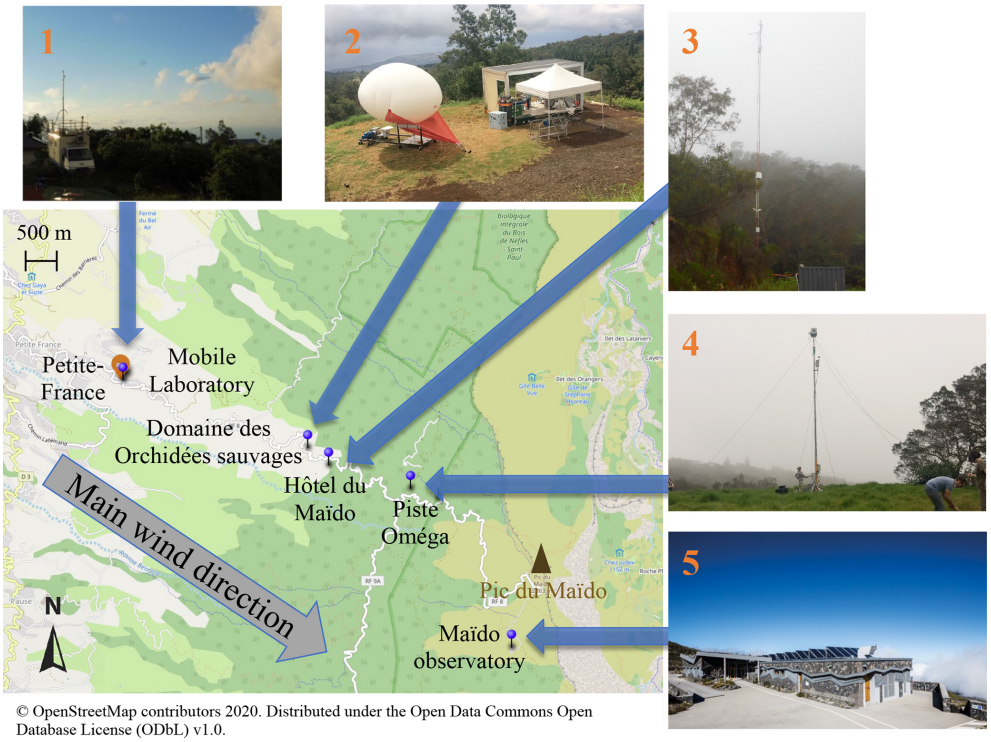

Figure 1. Location of the five instrumented sites during the BIO-MAÏDO campaign. The grey arrow indicates one of the two main paths for the dominant wind direction. Each site is illustrated with a photograph.

morning, the tethered balloon was operated in clear sky with an aerosol probe, whereas it was operated with cloud sensors at the end of the morning, when cloud appeared. The tethered balloon was operated for 21 d for 144 h of measurements. Following Fathalli et al. (2022), the adopted strategy was to alternate vertical soundings and levels at a constant altitude (20 min for turbulence or 5 to 10 min for cloud microphysics statistical representativeness) for each flight. Table 2 summarizes the instruments deployed at DOS-2 and the associated measured parameters.

2.4 Hôtel du Maïdo (HM-3): a forest area dedicated to flux measurements

HM-3 (1500 m a.s.l.; 21°03′16.4″ S, 55°21′21.4″ E) is a former holiday camp located in the middle of the forest. This site was dedicated to measurements of VOC fluxes. A 24 m instrumented mast and a container had been installed on the site. Several devices were deployed on the top of the mast: an ultrasonic anemometer including a temperature probe and an analyzer of carbon dioxide and water vapor. An inlet connected to a pump inside the container had also been installed at the top of the mast. This inlet brought air inside the container to several devices: a second analyzer of carbon dioxide and water vapor, an ozone analyzer, a PTR time-of-flight mass spectrometer (ToF-MS) for VOC measurements and active sampling on sorbent cartridges. The comparison of measurements from both analyzers of carbon dioxide and water vapor allowed estimation of the effects of the inlet on other chemical compound measurements inside the container. Measurements of the mixing ratio of biogenic organic compounds (isoprene and monoterpenes) by PTR-ToF-MS at 5 Hz were used to estimate their emissions thanks to the ultrasonic anemometer by eddy covariance. Finally, measurements of shortwave and longwave, upward and downward radiative fluxes as well as visibility and photosynthetically active radiation (PAR) were operated at the bottom part of the mast. Table 3 summarizes the instruments deployed at HM-3 and the associated measured parameters.

2.5 Piste Omega (PO-4): a forest site to sample cloud water

PO-4 (1760 m a.s.l.; 21°03′26.8″ S, 55°22′05.0″ E) is a forest trail from the Maïdo road. The site is surrounded by forest. A 10 m mobile mast was used to install a cloud impactor (see Fig. 1). This collector faced the slope from which the cloud came. A modified cloud droplet probe (CDP) was fixed on the mast just under the cloud collector to monitor the cloud microphysical properties. It measures the droplet size distribution from 2 to 50 µm in diameter, enabling the calculation of the liquid water content (LWC) and the effective diameter (D_{eff}). A meteorological station was also fixed on the mast (T, RH, wind speed). Finally, the AEROVOCC sampler was

Table 1. Instrumentation deployed at PF-1 and the associated measured parameters.

Instrument	Measured parameter	Sampling frequency	Institution in charge
Ultrasonic wind sensor Windsonic, Gill Instruments	Wind	15 min	Atmo-Réunion
Humidity and temperature sensor EE210, E+E Elektronik GmbH	Temperature, relative humidity	15 min	Atmo-Réunion
CO analyzer T300, Teledyne API	Mixing ratio of CO	15 min	Atmo-Réunion
Ozone analyzer O342M, Environnement SA	Mixing ratio of O_3	15 min	Atmo-Réunion
$NO/NO_2/NO_x$ analyzer T200, Teledyne API	Mixing ratio of NO, NO_2 and NO_x	15 min	Atmo-Réunion
SO_2 analyzer 43i, Thermo Fisher Scientific Inc.	Mixing ratio of SO_2	15 min	Atmo-Réunion
PTR-QMS, Ionicon Analytik GmbH	Mixing ratio of COV	1 min	LSCE
Aerolaser AL4021, Aero-Laser GmbH	Mixing ratio of HCHO	1 min	LaMP
		28 March–April	
Condensation particle counter MAGIC CPC, Aerosol Devices Inc.	Number concentrations of particles with diameters from 5 nm to 2.5 µm	10 s	Atmo-Réunion
High-volume sampler (Hi-VOL) Digitel DA80,	PM_{10} mass chemical concentration	Day and night	IGE
Megatec – filter	and bacterial diversity	10–12 h	
PQS1 radiometer, Kipp & Zonen	Photosynthetically active radiation (PAR)	15 min	CNRM
Ceilometer CT25K, Vaisala	Cloud base height	1 min	LACy
	Backscatter profile	1 min	

installed on the side of the cloud collector. AEROVOCC was developed to sample VOCs and OVOCs in cloudy air. It consists of three sorbent cartridges connected to three automated pumps to control samples at a constant flow.

During the whole campaign, 14 cloud water samples were collected (named R1 to R14 hereafter). The mean volume of the samplers was 111 mL. The sampled cloud water was further analyzed in the lab for (1) pH; (2) the main inorganic ions by ionic chromatography; (3) total organic carbon (TOC) by a TOC analyzer; (4) targeted organic compounds by high-performance liquid chromatography (HPLC)–mass spectrometry (MS) for carboxylic acids, by HPLC with fluorescence detection (HPLC-Fluo) for carbonyl compounds, by HPLC high-resolution mass spectrometry (LC-HRMS) for amino acids, by HPLC with a pulsed amperometric detector (HPLC-PAD) for sugars, and by stir bar sorptive extraction (SBSE) coupled to gas chromatography mass spectrometry (GC-MS) for low-solubility VOCs; and (5) hydrogen peroxide by derivatization and spectrofluorescence and Fe(II) and Fe(III) by complexation and ultraviolet–visible spectrophotometry (with a UV–Vis spectrophotometer). When enough volume of water was available, a non-target analysis was performed to investigate the complexity of the dissolved organic matter. Three clouds were analyzed by Fourier transform ion cyclotron resonance mass spectrometry (FT-ICR MS) using ionization in positive and negative polarities and multiple ionization sources to get a full picture of the composition of organic matter.

Viable culturable bacteria were investigated by culture platting of 0.1 mL of water samples on R2A medium and incubation at 25 °C in the dark. Colonies were isolated and taxonomically identified based on full-length 16S rRNA gene sequences, obtained from PCR amplification using the primers 27f and 1492r, and online Basic Local Alignment Search Tool (BLAST) software available from the National Center for the Biotechnology Information (NCBI) website, as in Vaïtilingom et al. (2012). Table 4 summarizes the instruments deployed at PO-4 and the associated measured parameters.

2.6 Maïdo Observatory (MO-5): a receptor site to observe the process air mass

MO-5 (2165 m a.s.l.; 21°04′46″ S, 55°22′59″ E) is surrounded by mountain shrublands. Previous simulations with the 3D Meso-NH model showed the vanishing of clouds at the same period of the year as the campaign at the observatory altitude (Duflot et al., 2019).

Table 2. Instrumentation deployed at DOS-2 and the associated measured parameters.

Instrument	Measured parameter	Sampling frequency	Institution in charge
Condensation particle counter CPC3788, TSI	Total number concentration of aerosols with diameters from 2.5 nm to 2.5 µm	1 s	CNRM
Scanning mobility particle sizer SMP3080, TSI	Size spectrum of aerosols with diameters from 10 to 500 nm	3 min	CNRM
Optical particle sizer OPC3330, TSI	Size spectrum of aerosols with diameters from 0.3 to 10 µm	5 min	CNRM
CCNC, Droplet Measurement Technologies	Number concentration of CCN at $S = 0.1\,\%$, $0.2\,\%$ and $0.3\,\%$	5 min for each supersaturation	CNRM
Fog monitor, Droplet Measurement Technologies	Size spectrum of droplets with diameters from 2 to 50 µm	1 s	CNRM
Present weather detector PWD22, Vaisala	Visibility	15 s	CNRM
	Rain	15 s	
	Luminance	15 s	
MARLEY lidar	Backscatter profile	1 min	LACy
Ceilometer CS135, Campbell Scientific	Cloud base height	10 s	LACy
	Backscatter profile	10 s	
Tethered balloon			
Optical particle counter (OPC), MetOne	Size spectrum of aerosols with diameters from 0.5 to 10 µm	6 s	CNRM
Cloud droplet probe (CDP), Droplet Measurement Technologies	Size spectrum of droplets with diameters from 2 to 50 µm	1 s	CNRM
Sonic anemometer	Wind	20 Hz	CNRM
	Temperature	20 Hz	
	Relative humidity	20 Hz	

Maïdo Observatory (Baray et al., 2013) can host atmospheric scientific experiments and offer the possibility for scientists to stay on site. Several European and international observation services operate at the observatory, and associated routine observations are done that in particular are of interest for BIO-MAÏDO: for aerosols (submicron size distribution, CCN concentration and total $PM_{2.5}$ number concentration), for gases (mixing ratio of ozone, nitrogen oxides, carbon monoxide and sulfur dioxide) and basic meteorological parameters. The BIO-MAÏDO campaign also benefited from the 2-year presence (October 2017 to November 2019) at the observatory of the high-sensitivity quadrupole-based PTR-MS of BIRA-IASB as part of the OCTAVE project. This suite of instruments was complemented by the online chemical characterization of nonrefractory PM_1 using the ToF ACSM, by PM_{10} filter sampling using a high-volume sampler identical to those deployed at PF-1 (Dominutti et al., 2022a) and by the same set of instruments deployed at DOS-2 to characterize the microphysical properties of clouds. The chemical and biological analyses of PM_{10} performed from filters are the same as at PF-1. The MO-5 station is also part of the ACTRIS (Aerosol, Clouds and Trace Gases Research Infrastructure) monitoring network and monitors the aerosol size distribution and number concentration using a custom-made differential mobility particle sizer (DMPS) with a commercially available condensation particle counter (CPC, TSI). Table 5 summarizes the instruments deployed at MO-5 and the associated measured parameters.

3 The main results

A large range of data was collected during the BIO-MAÏDO campaign. The cloud water collector deployed at PO-4 (Dominutti et al., 2022b) allowed more efficient sampling of cloud droplets than during the Forests gAses aeRosols Clouds Exploratory (FARCE) campaign (Duflot et al., 2019).

Table 3. Instrumentation deployed at HM-3 and the associated measured parameters.

Instrument	Measured parameter	Sampling frequency	Institution in charge
3D sonic anemometer CSAT 3, Campbell Scientific	Wind, temperature, relative humidity	10 Hz	LAERO
LI-7500 open-path gas analyzer, LI-COR	Mixing ratio of CO_2 and H_2O (mast)	10 Hz	LAERO
CNR4 radiometer, Kipp & Zonen	Up and down, longwave and shortwave radiations	1 min	LAERO
Present weather detector PWD22, Vaisala	Visibility	15 s	CNRM
	Rain	15 s	
	Luminance	15 s	
PQS1 radiometer, Kipp & Zonen	PAR	1 min	LAERO
LI-6262 closed-path gas analyzer, LI-COR	Mixing ratio of CO_2 and H_2O (container)	10 Hz	LAERO
O_3 analyzer TEI49i, Thermo Fisher Scientific Inc.	Mixing ratio of O_3	5 min	LAERO
PTR-ToF-MS 1000 ultra, IONICON	Mixing ratio of VOCs	5 Hz	LAERO
Smart Automatic Sampling System (SASS)	Mixing ratio of VOCs	Five cartridges per day 18 March–5 April	LaMP

Table 4. Instrumentation deployed at PO-4 and the associated measured parameters.

Instrument	Measured parameter	Sampling frequency	Institution in charge
Meteorological station	Wind, temperature	1 min	CNRM
	Pressure, relative humidity		
Cloud drop probe (CDP), Droplet Measurement Technologies	Size spectrum of droplets with diameters from 2 to 50 µm	1 s	CNRM
AEROVOCC	Mixing ratio of VOCs and OVOCs	One sample by event	LaMP
Cloud impactor	Chemical composition of cloud water	Duration of the event	LaMP
	Viable bacteria diversity		

Table S1 in the Supplement summarizes the daily operation of all the instruments deployed during the campaign. This report has been used to identify the days with the maximum amount of information available.

3.1 Meteorological overview of the campaign

The meteorological environment of Réunion (Réchou et al., 2019), and particularly of the Maïdo area, has been extensively studied in recent years in the framework of many measurement campaigns performed at Maïdo Observatory. Lesouëf et al. (2011), Guilpart et al. (2017) and Foucart et al. (2018) highlighted the main local and regional circulations that affect measurements at the observatory. Lesouef et al. (2013) and Duflot et al. (2019) studied the evolution of the mixing boundary layer and highlighted the superposition of several stratified layers along the Maïdo slopes. These previous results are summarized below.

For the main meteorological circulations that affect the campaign area, Réunion is subject to a strong easterly and southeasterly trade wind flow in winter and a weaker one in summer in the lowest layers of the atmosphere when the intertropical convection zone is close to Réunion. The Maïdo region located to the northwest of the island is conditioned by the convergence of two distinct flows: (i) the overflow regime due to the lifting of the trade winds over the topography of the island. This flow mainly affects the free troposphere; (ii) the counterflow regime corresponds to the circumvention of the trade winds around the topography. This low- and mid-altitude flow leads to a return flow generally located in the western and northwestern sectors downwind of the island.

Table 5. Instrumentation deployed at MO-5 and the associated measured parameters.

Instrument	Measured parameter	Sampling frequency	Institution in charge
Fourier transform infrared (FTIR) spectroscope	Wind, temperature	1 min	OPAR/BIRA-IASB
	Pressure, relative humidity		
CO analyzer Horiba	Mixing ratio of CO	1 min	OPAR
O_3 analyzer TEI49i, Thermo Fisher Scientific Inc.	Mixing ratio of O_3	1 min	OPAR
NO_x analyzer, Environnement SA AC31M	Mixing ratio of NO_x, NO and NO_2	1 min	OPAR
SO_2 analyzer T421, Thermo Fisher Scientific Inc.	Mixing ratio of SO_2	1 min	OPAR
Condensation particle counter CPC3776, TSI	Number concentration of particles with diameters from 25 nm to 1 µm	10 s	OPAR
Custom-made differential mobility particle sizer with a condensation particle counter CPC3100, TSI	Size spectrum of aerosols with diameters from 13.7 to 650 nm, 14 size classes	8 min	OPAR/LaMP
Aerosol chemical speciation monitor ToF-ACSM, Aerodyne Research Inc.	Chemical composition of NR-PM_1	10 min	LaMP
High-volume sampler (Hi-VOL) Digitel DA80, Megatec – filter	PM_{10} mass chemical concentration and biological composition	Day and night 10–12 h	IGE
PTR-MS, Ionicon Analytik GmbH	Mixing ratio of VOCs	2.7 min	BIRA-IASB
Aerolaser AL4021, Aero-Laser GmbH	Mixing ratio of HCHO	1 min 13–27 March	LaMP
Fog monitor, Droplet Measurement Technologies	Size spectrum of droplets with diameters from 2 to 50 µm	1 s	CNRM
Present weather detector PWD22, Vaisala	Visibility	15 s	CNRM
	Rain	15 s	
	Luminance	15 s	

More locally, thermal breezes strongly influence the weather during the daytime: near the coast, sea or land breezes are formed, and higher up, anabatic or catabatic breezes affect the slopes during the day or night. All these circulations lead to ascents on the slopes of Maïdo almost daily, with cloud formation in the middle of the morning and at the beginning of the afternoon, followed by subsidence and stratification of the boundary layer leading to the evaporation of the clouds at the end of the daytime. Maïdo Observatory is generally located in the trade wind overflow flow, except in the middle of the day, when it is located close to a convergence zone between the overflow flow and the thermal ascents on the slopes. At night, the observatory is located in the free troposphere.

These different mechanisms have mainly been highlighted by numerical modeling and on case studies lasting a few days. The availability of two meteorological stations located at PF-1 (mid-slope) and MO-5 (summit) during the BIO-MAÏDO campaign made it possible for the first time to characterize thermal breezes on the Maïdo slope over a period of 27 d corresponding to the transition period between the wet season and the dry season.

The weather conditions observed during the campaign are summarized by the wind roses resulting from local observations in Fig. 2. Figure 2a and b correspond to the wind observed at PF-1 and MO-5 between 14:00 and 04:00 UTC (i.e., from the end of the afternoon to the beginning of the morning). At both stations, the wind regime is from the south and southeast, with a maximum wind speed between 2 and 3 $m\,s^{-1}$ at PF-1 (frequency 35 %) and higher than 4 $m\,s^{-1}$ at MO-5 (frequency 15 %). These conditions show the strong influence of the trade winds and the overflow conditions at night. The wind conditions observed during the daytime (from 04:00 to 18:00 UTC; Fig. 2c and d) are more variable, especially at MO-5. At PF-1, the flow is essentially from the west (30 %) and of a lower intensity than at MO-5 (generally

between 1 and 3 m s^{-1}). This direction is typical of the upward flow of the air mass on the slopes by thermal breezes or the return flow of the trade winds. At MO-5, the air masses have two opposite directions: from the north (14 %) to the east (8 %) and from the south (6 %) to the west (20 %). This indicates a reversal of the wind direction during the daytime, as observed by Rocco et al. (2022). These conditions were consistent with the period of transition from the wet to dry seasons.

Verreyken et al. (2020, 2021) and Rocco et al. (2020) studied the origin of the air masses measured at Maïdo Observatory by using Lagrangian trajectory tools (FLEXPART, CAT). Their results concerned the origin of air masses from the atmospheric transport at the synoptic scale and showed that the dominant large-scale air masses are easterly under the influence of trade winds and that the strongest biogenic contributions coincided with air masses passing over the northeastern part of Réunion. For the BIO-MÄIDO campaign, to determine the origin of the air masses arriving at PF-1 and MO at the scale of the entire island, high spatiotemporal back-trajectories have been calculated using Meso-CAT. The used Meso-NH simulations cover the whole campaign and use three embedded domains at 2 km, 500 m, and 100 m horizontal resolutions. Rocco et al. (2022) first exploited these back-trajectories by combining them with soil data from the Corine 2018 land cover database (European Environment Agency, 2020) to assess the origin of the air masses sampled at MO. Moreover, the dominant circulations schemes at the scale of the highland are better highlighted by new elements provided here and obtained by calculating footprint maps using Meso-CAT in back-trajectory mode.

Figure 3 gives the footprint of PF-1 and MO-5 using back-trajectories of Meso-CAT from the 500 m of the horizontal-resolution domain. These footprints are computed by assembling all the back-trajectories that reached these two stations and by counting all the trajectory points per pixel of 1 km size. Two types of footprints have been calculated, the first of which corresponds to the total atmospheric column, keeping all the trajectory points (Fig. 3a and b), and the second where we select only the trajectory points located at less than 500 m a.g.l. and during midday (between 06:00 and 14:00 UTC; Fig. 3c and d).

The total column footprint of PF-1 (Fig. 3a) clearly shows the influence of the trade winds with air masses arriving from the southeast, bypassing the island of Réunion as much from the north as from the south and generally arriving on PF-1 with an ascent by the slopes. These air masses are well channeled and bypass the topography by the southern flank of Réunion. The main part of the back-trajectories arrives locally from the west and is more variable and diffuse over the whole campaign period. At MO-5 (Fig. 3b), there is a wider dispersion of air mass origins. The signature of the trade winds is even more visible, with air masses generally arriving more directly at MO-5 and mainly passing through the south. The footprint also shows more trajectory points east of MO-5, indicating the influence of frequent ascents of air masses from the Cirque de Mafate.

To study the mixing boundary layer air masses advected by thermal breezes, other footprints have been calculated according to the following criteria: (i) only the back-trajectories remaining in the mixing boundary layer arbitrarily set as a 500 m (above ground level) thick layer are kept; (ii) we have retained the periods of the day when there are back-trajectories coming from the southwest to the northwest between 06:00 and 14:00 UTC (Fig. 3c and d). Again, two preferred trajectory routes can be seen for PF-1 and for MO-5, the main part of the air masses passing through the south. This means that the PF-1 measurements were able to load themselves with chemical and biological compounds over the forests located between 1000 and 1500 m a.s.l. in the southwest of the island. The other well-marked result is the one going up the western flank of the island, whose trajectories also show a passage in the marine boundary layer. Through differences with the total day integration, one can note that most of the back-trajectories modeled at MO-5 come from the south to the northwest, which corresponds to the return branches of the trade winds associated with the upslope thermal breezes.

The connection between MO-5 and the other observation sites of the campaign is clearly evidenced by the footprints. This is consistent with the high dynamic correction occurrence computed by Rocco et al. (2022, Fig. 4c) for almost each day of the campaign. As for PF-1, several trajectories also indicate an origin of the marine boundary layer. These specific periods will be studied preferentially to follow the Lagrangian evolution of the chemical composition of the air mass.

3.2 Dynamical context for a typical cloudy day

An example of the dynamical context of the BIO-MAÏDO measurements is provided on 28 March 2019. Using back-trajectories and forward-trajectories computed with Meso-CAT, Rocco et al. (2022) and Dominutti et al. (2022b) were able to show that this situation was typical and highlighted the good connection between the observation sites.

Figure 4 shows the temporal evolution of the simulated low-level dynamics for the day of 28 March 2019 (500 m domain). The upper figures show the wind direction (color and vector) and intensity (vector size) at the surface at 03:00 UTC (a) and 08:00 UTC (b). During this day, the trade wind flow at the surface has a southeastern component slightly disturbed by the presence of Cyclone Joaninha located about 1000 km southeast of Réunion. Larger temporal- (120 h) and spatial-scale (the domain covers 40 to 75° E) 5 d back-trajectories calculated with CAT and ERA5 ECMWF wind fields show that, on 28 March, the air masses arriving at Réunion came from the active area of the cyclone whose center is located near 15° S, 60° E on 24 March (see Supplement Fig. S1).

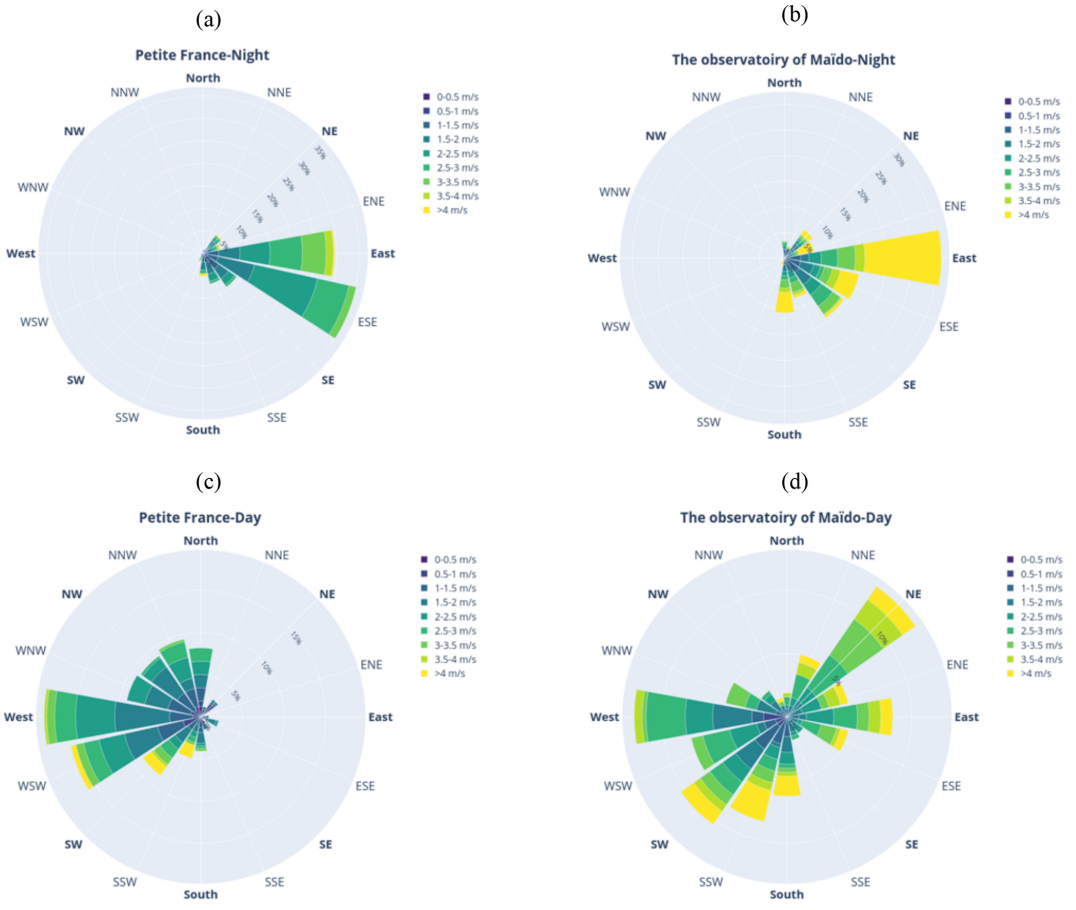

Figure 2. Wind rose at PF-1 and MO-5 between 14:00 and 04:00 UTC (nighttime; **a**, **b**) and from 04:00 to 18:00 UTC (daytime; **c**, **d**) averaged over the entire campaign from 11 March to 7 April. The intensity is in meters per second.

Classically, the trade wind flow bypasses the topography of Réunion with two zones of wind acceleration off the southwestern and northeastern coasts of the island. At the very beginning of the morning (03:00 UTC), the trade wind return loop is located in the north of the island. This circulation does not penetrate inland (Fig. 4a).

At 08:00 UTC, the trade wind return loop moved northwest. There is a significant penetration of this surface flow as far as the DOS-2 station. MO-5 is located in a convergence zone between the overflow trade wind flow and this northwesterly counterflow (Fig. 4b). The cloud water content integrated on the vertical is represented in grey. No cloud formation is modeled at 03:00 UTC, apart from a few orographic clouds due to the uplift of the trade winds on the southern flank of the Piton de la Fournaise volcano. Over the BIO-MAÏDO area, the sky is clear (Fig. 4a). At 08:00 UTC associated with the ascent of the wind flow above the slopes of the Maïdo area, an important formation of clouds is stimulated. All the northwest of the island is affected by the presence of clouds between 1000 and 2000 m a.s.l. (Fig. 4b).

A vertical cross section (Fig. 4c and d) has been made on the axis of the red line of Fig. 4a and b. This cross section has used the simulation results from the 100 m horizontal resolution domain at 03:00 and 08:00 UTC. At 03:00 UTC (Fig. 4c), it can be seen that three wind layers have been modeled. Close to the surface, a catabatic wind flow is modeled along the slope. At about 500 m a.g.l., a wind shear is modeled, and the airflow came from the northwest. This last layer is attributable to the return loop of the trade winds. Above, at about 2500 m a.g.l., the wind direction is southeast due to the trade wind overflow above the island.

At noon (08:00 UTC), the anabatic thermal breeze is clearly modeled. This wind regime is added with the trade wind return loop on a 1 km thick layer (Fig. 4d). This upward flow flux reaches 2000 m a.s.l., and we find again in the MO-5 area the convergence zone due to the trade wind overflow. As seen before, clouds are simulated over the slopes of the Maïdo area. This presence of clouds affects almost the entire simulation domain (i.e., between 500 and 2400 m a.s.l.). The base of the clouds reaches the surface between 700 and 1900 m a.s.l. and therefore an area covering all the measurement sites except MO-5. Figure 4e shows the time series of the MARLEY backscattered signal at the DOS-2 site for 28 March until 08:15:00 UTC (the system failed after-

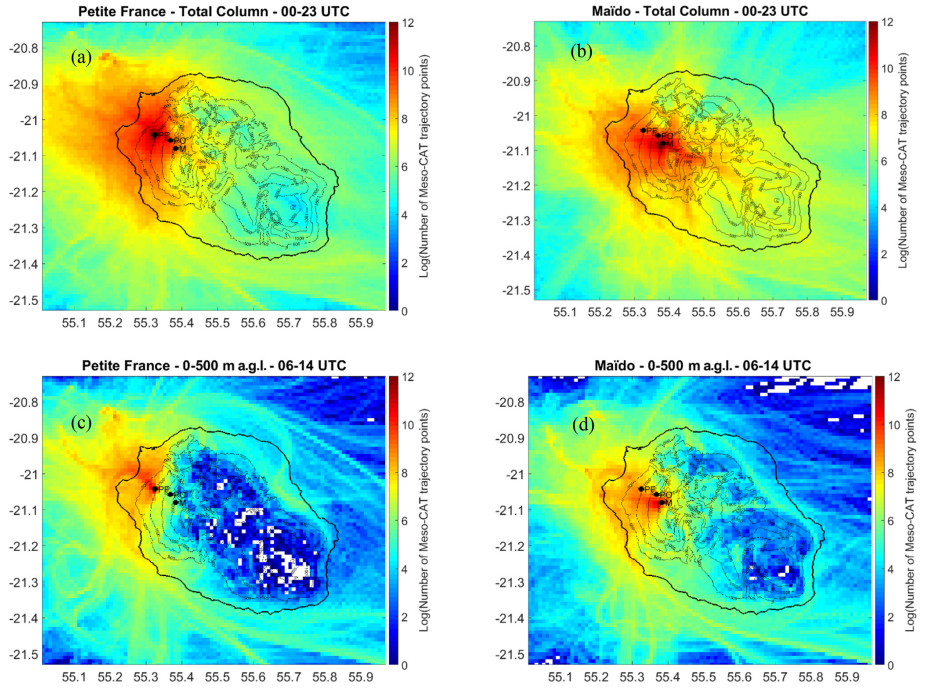

Figure 3. Natural logarithm of the number of back-trajectory points arriving at Petite France **(a, c)** and Maïdo **(b, d)** from 15 March to 8 April per scare of 0.01° (around 1 km) size. All trajectory points are taken into account for the calculation of the total column footprint maps **(a, b)**, but only trajectory points during the midday (between 06:00 and 14:00 UTC) and between the ground and 500 m a.g.l. for the near-surface footprint maps **(c, d)**.

wards due to a power supply failure). The sky is clear until 06:00 UTC, when the formation of clouds is triggered. The cloud base reaches the surface and the cloud top reaches 2200 m a.s.l. These observations validate the simulated formation of clouds at DOS-2. Due to the dynamical transport above the slopes, these simulation results indicate that the air mass may have been loaded with chemical compounds in the aqueous phase before being evaporated near MO-5.

3.3 VOC measurements

During the BIO-MAÏDO campaign, three PTR-MSs were simultaneously installed for the first time in a tropical area to perform VOC mixing ratio measurements along the slope of the Maïdo road at PF-1, HM-3 and MO-5. In addition, during this campaign, characterization of VOC emissions from tropical and endemic, indigenous and exotic vegetation has been accomplished using solid sorbent cartridges for sampling followed by an analysis with the gas chromatography mass spectrometer and by the eddy covariance method and PTR-ToF-MS measurements at the HM-3 site.

VOC measurements were first performed during the FARCE campaign in 2015 on Réunion (Duflot et al., 2019); concentrations of isoprene were measured in different locations of the island. In this study, the maximal concentrations of isoprene were measured in the 100 to 200 pptv range at the tropical forest site (Bélouve Forest). From 2018 to 2021, a PTR-MS was installed at MO-5 for continuous VOC measurements as part of the OCTAVE project. These measures were used in Verreyken et al. (2020), who addressed the impact of long-range biomass burning at the remote site of MO-5, and an overview of the 2-year campaign is presented in Verreyken et al. (2021). In this last study, high levels of BVOCs were observed and isoprene concentrations reached up to 500 pptv. In addition, during the OCTAVE project, a second PTR-MS was positioned at the Bélouve Forest (20.9° S, 55.3° E; 7 m a.s.l.) and Le Port (21.06° S, 55.5° E; 1498 m a.s.l.) sites for 10 d each in April–May 2018. In a study dedicated to the analysis of formaldehyde sources and origins at MO-5 using these additional measurements, Rocco et al. (2020) found that most of the formaldehyde is formed from biogenic secondary compounds (oxidation of biogenic VOCs with 37 % on average).

Figure 5 compares averaged mixing ratios of isoprene, terpenes and BTEX (sum of benzene, toluene, ethylbenzene and xylenes) at MO-5 for four datasets corresponding to the FARCE, OCTAVE-1 (first – 2018 datasets), BIO-MAÏDO and OCTAVE-2 (2018 and 2019 datasets) campaigns. The dominant mixing ratios are observed for isoprene all over the different campaigns with an averaged concentration of 95 ± 133 pptv. Low mixing ratios of terpenes and BTEX are measured at MO-5, showing low influence of anthropogenic emissions and low emissions of monoterpenes by local vegetation. Levels of isoprene are higher for BIO-MAÏDO and

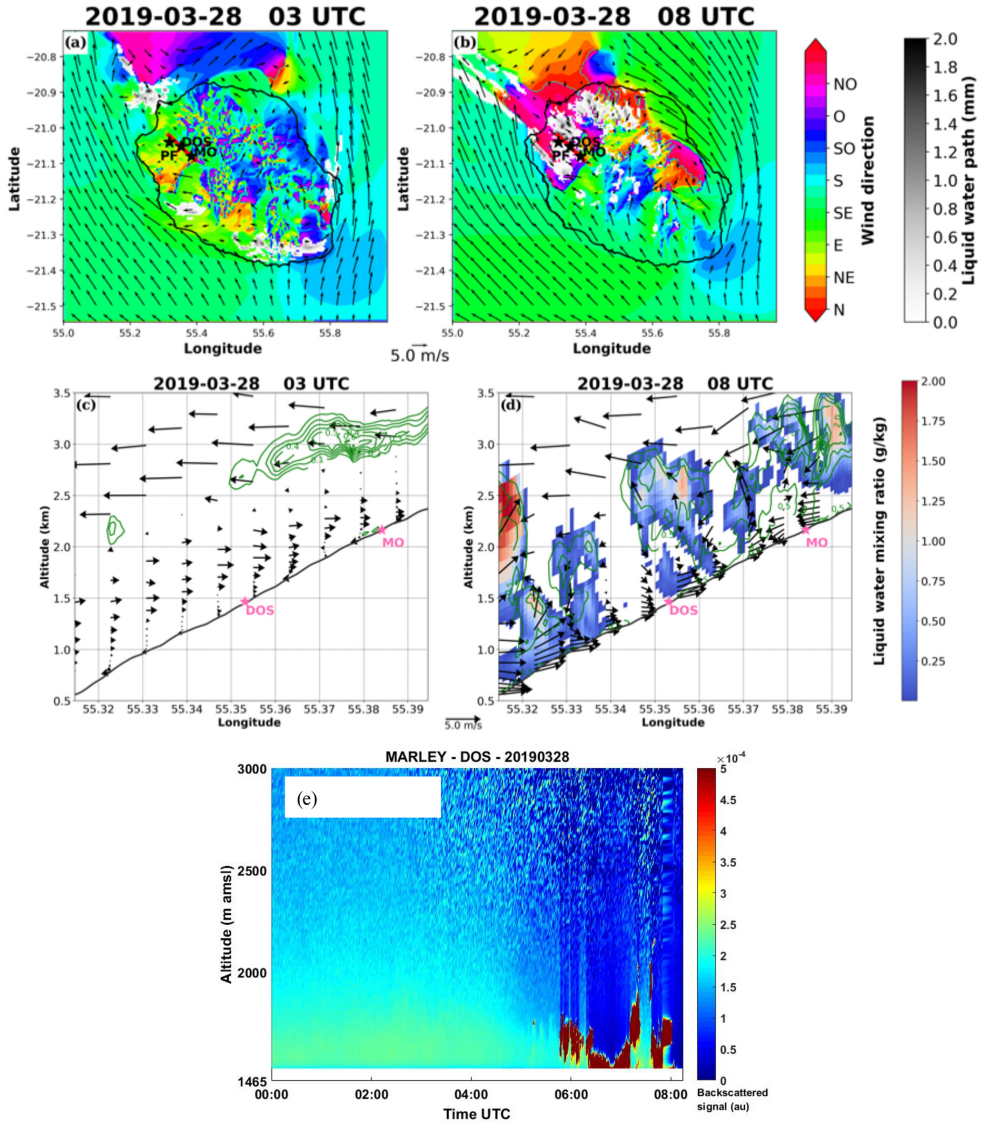

Figure 4. Meso-NH simulation: **(a, b)** horizontal cross section at the surface for wind direction (color scale) and intensity (vector in meters per second) and liquid water path (mm, in grey) at 02:00 UTC **(a)** and 08:00 UTC **(b)** for 28 March; **(c, d)** vertical cross section along the red line superposed on panels **(a)** and **(b)** showing the liquid water mixing ratio (color scale in grams per kilogram), wind direction and intensity (vector in meters per second) and turbulent kinetic energy (TKE) (green isoline in meters per square second) at 02:00 UTC **(c)** and 08:00 UTC **(d)** for 28 March. **(e)** MARLEY backscattered signals at DOS-2 for 28 March.

the second set of OCTAVE than for FARCE and the first set of OCTAVE. For the FARCE campaign, terpenes and BTEX are not available. Terpenes are highest for BIO-MAÏDO and lowest for BTEX, but with levels comparable to the other datasets.

The coupling of VOC chemistry and dynamics measured during the BIO-MAÏDO campaign was investigated to better understand the role of dynamics in the distribution of VOCs (Rocco et al., 2022). This new and first approach combined land cover footprints and back-trajectories. It provided information on the nature of the ground surface influencing the air masses during the few days and hours before the air mass arrives at the sampling sites (PF-1 and MO-5). The variability of VOC concentrations along the slope was also analyzed. The origin of air masses greatly varied among the days. It showed differences in forward trajectories and back-trajectories coming from PF-1 to MO-5 with air masses more or less advected from the downslope areas. Many days were marked by a frequent oceanic air mass origin (up to 50 %) with high concentrations of methanol and acetone. Ratios of isoprene oxidation products to the isoprene concentration have been calculated. The calculated ratios were on average 0.44 ± 0.42 at MO-5 and 1.11 ± 1.59 at PF-1. A lower ratio at MO-5 indicates recent emissions of isoprene and therefore

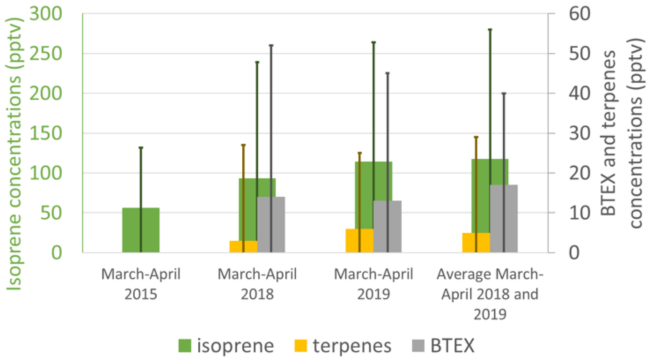

Figure 5. Isoprene, terpenes and BTEX mixing ratio (pptv) for the FARCE campaign (March–April 2015, Duflot et al., 2019), OCTAVE-1 campaign (March–April 2018, Rocco et al., 2020), BIO-MAÏDO campaign (March–April 2019, Rocco et al., 2022) and OCTAVE-2 campaign (March–April 2018–2019, Amelynck et al., 2021) at the Maïdo Observatory.

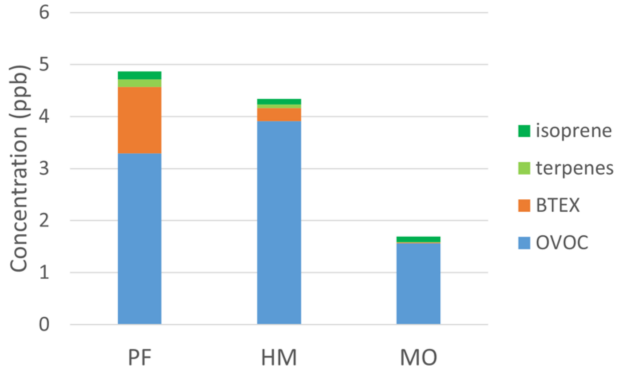

Figure 6. Average concentration of isoprene, terpenes, OVOCs and the BTEX concentration in parts per billion at Petite France (PF-1), Hotel du Maïdo (HM-3) and Maïdo Observatory (MO-5).

a major contribution from the local vegetation, which has not yet had time to oxidize to secondary compounds.

Figure 6 shows the average composition of the isoprene, terpenes, OVOCs (sum of methanol, acetaldehyde, acetone and methyl ethyl ketone – MEK) and BTEX mixing ratios at PF-1, HM-3 and MO-5 averaged during the whole BIO-MAÏDO campaign. A spatial gradient in the total VOC mixing ratios is observed from PF-1 to MO-5 with a decrease by a factor of 2.5 between PF-1 and MO-5. OVOCs are the major contributors to the total VOC burden (> 50 % in volume), while the contribution becomes lower for primary biogenic and anthropogenic VOCs from PF-1 to MO-5, where OVOCs are dominant. This gradient depends on the distance to the main primary sources (i.e., vegetation and traffic), air mass history during its transport (cloud presence, surface characteristics) and air mass aging.

During the BIO-MAÏDO campaign, mixing ratios of isoprene measured at the three sites were between 100 and 600 pptv. The average isoprene mixing ratios for the period were 0.16 ± 0.12, 0.11 ± 0.10 and 0.12 ± 0.15 ppbv at PF-1, HM-3 and MO-5, respectively. Terpene mixing ratios are 20 times higher at PF-1 than at MO-5, reaching a value of 140 pptv. As PF-1 is a mixed rural and urban site, the sources of terpenes are more abundant at this site than at MO-5. At HM-3, averaged concentrations of α-pinene, β-pinene and limonene were, respectively, 0.06 ± 0.04, 0.01 ± 0.01 and 0.09 ± 0.05 ppbv. As a marker of anthropogenic emissions, BTEXs are also present at a higher level at PF-1 (1.27 ± 0.67 ppbv) than at MO-5 and HM-3. Dilution and oxidation processes explain the decreasing levels due to the increased distance to the source. Other hypotheses must be considered. Despite BTEX being poorly soluble in water, BTEX was detected in every cloud water sample with a mean concentration of 4.2 nM (Dominutti et al., 2022a), showing that clouds act as a sink for aromatic compounds. Another potential sink is the deposition of BTEX on the leaf cuticle through gaseous deposition (Molina et al., 2021). Finally, Rocco et al. (2022) showed that PF-1 and MO-5 were not dynamically connected every day during the campaign. Concerning the OVOCs, the species with higher mixing ratios for the three sites is methanol, with average mixing ratios of 2.16 ± 0.89, 2.79 ± 1.10 and 0.82 ± 0.35 ppbv at PF-1, HM-3 and MO-5, respectively. As this compound is primarily emitted by terrestrial plants during the growth and decay stages (Bates et al., 2021, and references therein), this can explain the highest mixing ratio observed at HM-3.

3.4 Aerosol measurements

During the BIO-MAÏDO campaign, an online ToF-ACSM, operating continuously from 13 March to 2 April, was used to determine the chemical composition of non-refractory PM_1 (NR-PM_1) aerosol at MO-5, providing mass concentrations for organic, sulfate, nitrate, ammonium and chloride species. Additionally, PM_{10} aerosols were simultaneously sampled by offline filters at MO-5 and PF-1 during the whole field campaign.

At MO-5, the average NR-PM_1 mass concentration was $4.6 \pm 6.2\ \mu g\ m^{-3}$ with a strong diurnal variability. Daily mass concentrations reaching up to $25\ \mu g\ m^{-3}$ were observed at the start and end of the field campaign, while nighttime concentrations, when the site was most likely in the free troposphere, were close to the limit of detection of the instrument. These measurements were coherent with aerosol number concentrations measured with a DMPS that showed similar diurnal profiles with typical signatures of new particle formation on a daily basis (Rose et al., 2019).

The NR-PM_1 was dominated by SO_4^{2-} (57.3 %), followed by organics (23.3 %), NH_4^+ (14.2 %) and NO_3^- (2.2 %) (Dominutti et al., 2022a). The high concentration of sulfate-containing particles and the low concentration of NH_4^+ show that forms of sulfate other than ammonium sulfate ($(NH_4)_2SO_4$) were sampled, likely acidic aerosol such as

NH_4HSO_4 or eventually in the form of organosulfates (Brito et al., 2018).

The contribution of different organic species to the total organic mass concentration was determined using positive mass factorization (PMF) with the source finder (SoFi) toolkit (Canonaco et al., 2013). PMF aims to solve a matrix equation using a weighted least-squares approach, which provides different factor profiles by testing rotational techniques available in the ME-2 engine. Different solutions from two to six factors were tested, and a final solution of three factors was chosen based on optimal Q/Q_{exp} values, physically meaningful reference profiles and time series. The three-factor solution was resolved using PMF analysis of the entire organic matrix from m/z 1 to 150: a MOOA (75 %), a primary organic aerosol (POA) (18.5 %) and an isoprene-derived organic aerosol (IEPOX-OA) (11 %), as fully described in Dominutti et al. (2022a). This solution characterized up to 80 % of the total organic aerosol fraction measured.

During the second part of the field campaign, air masses were exposed to aqueous-phase processing (as determined using the results of the Meso-NH model). Using this information, aerosol chemical composition and physical properties were compared under both clear and cloudy conditions. A clear shift in the aerosol size distribution was observed (an increase of 15 % of Aitken- and accumulation-mode aerosols under cloudy conditions) as well as a shift in the organic aerosol chemistry with increases in MOOAs, in oxalic acid concentrations and in sulfate aerosols in the PM_{10} offline filters. These observations together with model estimates of in-cloud processing of aerosols suggest that oxidation of gaseous precursors, primary organic aerosol species and other aqueous-phase processing has a significant impact on the sources of organic aerosol (notably oxalic acid) and on aerosol physical properties (Dominutti et al., 2022a).

Figure 7 presents the average concentrations of different PM_{10} components observed at MO-5 and PF-1 during the BIO-MAÏDO field campaign, split between daytime and nighttime. The main differences between both sites were observed for total organic matter (OM) concentrations, which were higher at PF-1 (3480 ng m^{-3}) than at MO-5 (1506 ng m^{-3}) by a factor of 2.3 (Fig. 7a and b). In addition, higher concentrations at PF-1 were also observed for Na^+ and NO_3^- (by a factor of 2) and for Cl^- and EC (by factors of 3.6 and 4.5, respectively) (Fig. 7a and b). These differences could be related to the distance of the sites from emission sources, as is the case for the marine origin ions Cl^- and Na^+ and the traffic-related ones EC and NO_3^-. On the other hand, sulfate and ammonium, being associated with long-range transport, do not differ significantly in the average concentrations of the sites. A second large difference comes from the fact that MO-5 is under free tropospheric conditions during the night, leading to much larger differences in the day–night ratios at MO-5 than at PF-1. Notably, OM at PF-1 does not show a substantial difference between daytime and nighttime (2.01 and 1.81 µg m^{-3}, respectively); however, its concentrations were dissimilar at MO-5 (0.90 and 0.35 µg m^{-3}, respectively).

The OM composition was also variable between the sites and also on a day–night basis (Fig. 7c). As expected, sugar alcohols and monosaccharides had higher concentrations at PF-1 than at MO-5, by a factor of 3 to 10. Mean concentrations at PF-1 were determined by arabitol (49 ng m^{-3}), levoglucosan (38.6 ng m^{-3}), mannitol (35.5 ng m^{-3}) and glycerol (19.3 ng m^{-3}). At MO-5, a similar profile is observed but is differently controlled by levoglucosan (8.8 ng m^{-3}), mannitol (6.5 ng m^{-3}), trehalose (4.9 ng m^{-3}) and arabitol (4.4 ng m^{-3}). Interestingly, higher concentrations of sugars were observed at night at PF-1 (Fig. 7c), suggesting that environmental conditions (such as temperature and humidity) can have a role in the emission processes of these compounds by natural sources (e.g., soils, bioaerosols, plants or fungal spores). Zhang et al. (2010) found that arabitol and mannitol in PM_{10} showed significant correlations with relative humidity and air temperature, suggesting a wet emission mechanism of biogenic aerosol in the form of fungal spores in a tropical rainforest. The sugar alcohols, mannitol and arabitol, are common energy reserves in fungi and are produced in large amounts by many fungi (Golly et al., 2019; Zhang et al., 2010; Bauer et al., 2008). In contrast, levoglucosan, a degradation product from biopolymers, is known as a good molecular tracer of biomass burning in the literature (Simoneit, 2002). However, levoglucosan concentrations observed in our study are more likely to be due to domestic biomass burning (e.g., cooking emissions) than forest fires (not reported in the area during the campaign). Thus, our results show a specific contribution of biogenic sources to PM_{10} samples such as fungi spores, soils or microorganisms and, to a lesser extent, the contribution from biomass aerosols.

Seventeen organic acid concentrations were measured at both sites (Fig. 8) from PM_{10} samples. In contrast to what was observed for ions and sugars, higher mean concentrations of total organic acids were obtained at MO-5 (95.3 ng m^{-3}) than at PF-1 (56.5 ng m^{-3}). The largest contribution at both sites was from oxalate, which presented average daytime concentrations of 63 ng m^{-3} at MO-5 and 15 ng m^{-3} at PF-1. Oxalic acid is the most abundant and ubiquitous dicarboxylic acid (Kawamura and Bikina, 2016) and is commonly classified as a secondary organic tracer formed from the photochemical and aqueous oxidation of many organic precursors (Ervens et al., 2011). As discussed by Dominutti et al. (2022a), the large contribution of this acid at MO-5 suggests the impact of more oxidized aerosols transported over long distances. Organic acids also include the presence of other dicarboxylic acids, such as malonic, malic and succinic, species typically observed in other and similar environments (Kawamura and Bikina, 2016; Golly et al., 2019; Cheng et al., 2013; Wang et al., 2006). The average daytime concentrations of malonic acid were similar at both

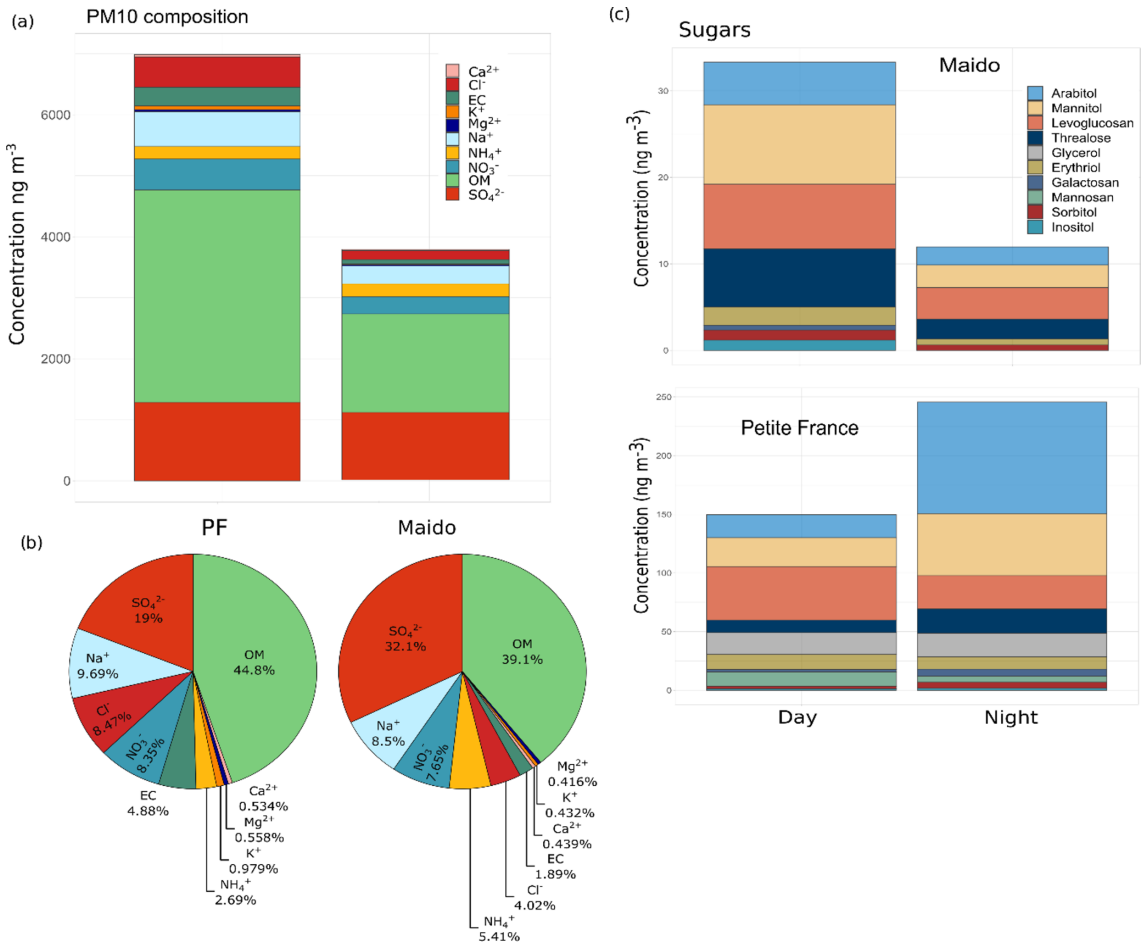

Figure 7. **(a)** Average PM_{10} composition observed at Petite France (PF-1) and Maïdo Observatory (MO-5), **(b)** relative contribution of PM_{10} components during daytime observations and **(c)** average sugar concentrations at the PF-1 and MO-5 sites during daytime and nighttime.

sites (15.6 and 12.1 ng m^{-3} at PF-1 and MO-5, respectively). However, succinic acid (5.9 and 9.6 ng m^{-3} at PF-1 and MO-5, respectively) and malic acid (10.4 and 4.2 ng m^{-3} at PF-1 and MO-5, respectively) exhibited some small differences between the sites. These acids can be emitted into the atmosphere from various anthropogenic (e.g., vehicle or biomass burning) and natural (marine aerosol) sources, but these are mainly produced in the atmosphere by several photochemical reactions of their organic precursors. The involvement of the photochemical process in the production of these acids can be evaluated by the mass ratio of malonic acid to succinic acid (> 1 for photochemically aged aerosols, Kawamura and Sakaguchi, 1999). Our observations show average malonic and succinic ratios of 2.62 and 1.51 at PF-1 and MO-5, respectively, confirming the presence of photochemically aged aerosols on Réunion.

Overall, the chemical profiles and PM_{10} concentrations show that the MO-5 and PF-1 sites are rather disconnected during most of the field campaign, especially at night. The results reveal that different environmental conditions and atmospheric dynamics have an impact on the spatial distribution and composition of aerosols on Réunion.

3.5 Cloud chemistry analysis

During the BIO-MAÏDO campaign, 14 cloud samples were collected at PO-4 and characterized by physicochemical and microbiological analysis. This section is devoted to summarizing the main results described in detail in Dominutti et al. (2022b) and to presenting the ongoing work.

Data obtained with the CDP reveal that clouds collected on the slope of the mountainous island present a low water content with LWC values of 0.07 ± 0.04 g m^{-3} on average. These values are more representative of the LWC reported for fogs than the higher ones reported for marine clouds (values closer to 0.2 to 0.4 g m^{-3}), such as those sampled at Puerto Rico (Gioda et al., 2013) or Cabo Verde (Triesch et al., 2021). This is the atmospheric dynamical circulation that leads to the formation of clouds with a low LWC over this part of the island (see Sect. 3.2 and Duflot et al., 2019). Concerning the

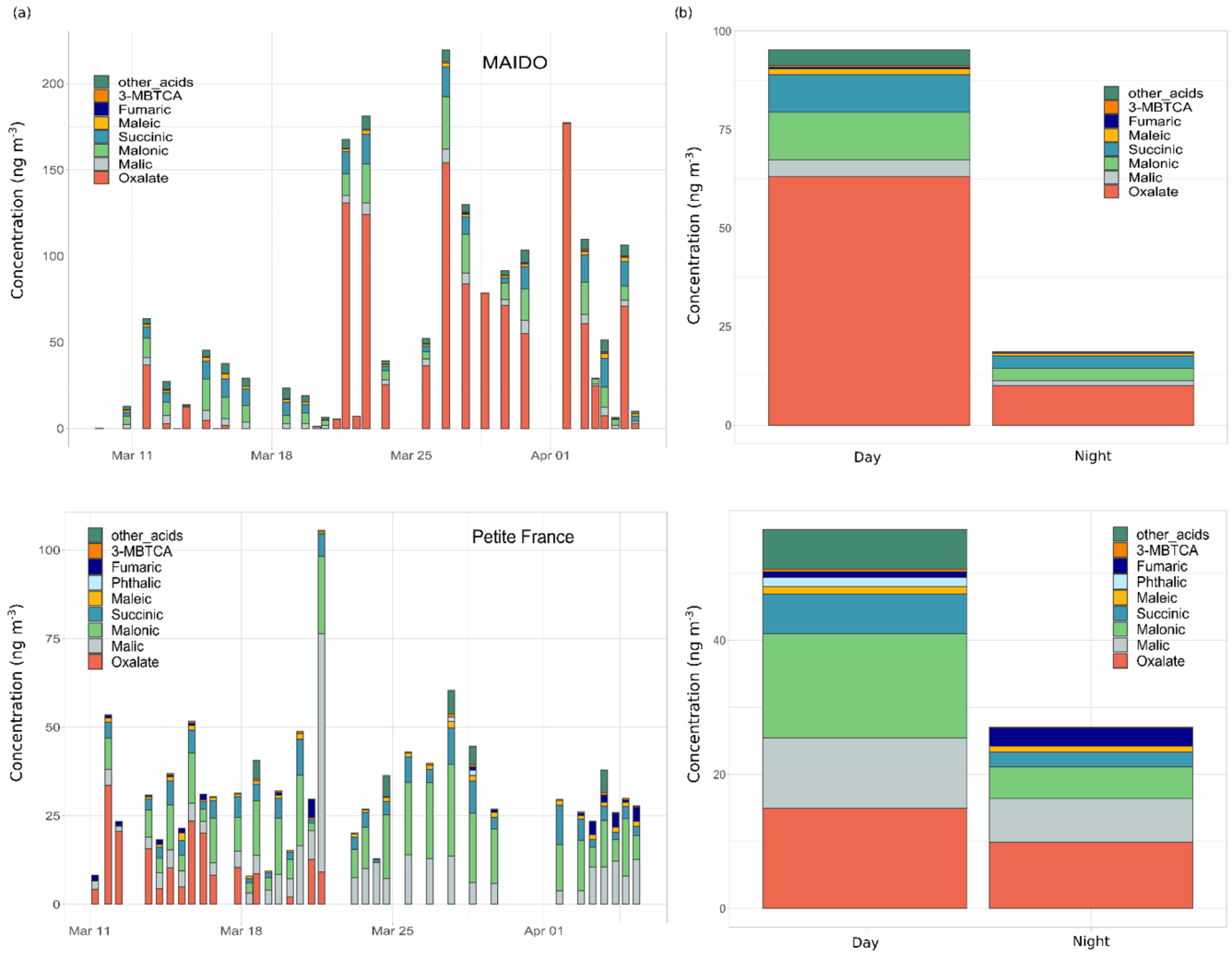

Figure 8. **(a)** Time series evolution of organic acid concentrations observed at MO-5 and PF-1 in PM_{10} and **(b)** average concentrations observed at each site during day and night observations.

size of the droplets, the D_{eff} for the 14 cloud events is rather small, with an average value of 13.7 ± 1.51 µm (Fig. 9a).

The main inorganic ions have been quantified in priority since they are used as tracers of various natural and anthropogenic sources (Deguillaume et al., 2014). In line with the low LWC, the total concentrations of these ions are a little diluted and therefore high, with concentrations ranging from 600 to 4370 µmol L^{-1}. As expected, for all the cloud events, a major influence of ions of marine origin is found, confirming the contribution of sea salt to the cloud formation (Na^+: 490 ± 399 µmol L^{-1}; Cl^-: 434 ± 370 µmol L^{-1}) (Fig. 9b). These amounts are similar to those observed for the other marine sites. Nitrates are the third ions in the relative contribution, with a concentration of 239 ± 168 µmol L^{-1}. These elevated concentrations may be linked to local anthropogenic sources (uptake of NO_x / nitric acid from the gas phase into the droplets or dissolution of nitrate from aerosols). This additional anthropogenic fraction is confirmed by the presence of sulfate in a significant quantity (118 ± 44 µmol L^{-1}). The measured SO_4^{2-}/Na^+ ratio is much higher than the standard sea salt molar ratio by a factor of 2.8 on average, confirming the anthropogenic contribution to the sulfate amount. The contribution to the sulfate concentration of volcanic emissions through the dissolution of SO_2 in cloud droplets and oxidation to form sulfates cannot be ignored, even if no eruption was reported during the sampling period. Ammonium levels (123 ± 43 µmol L^{-1}) are comparable to the observations conducted for remote continental sites, indicating plausible terrestrial or agricultural inputs. The concentration of these compounds determines the cloud water acidity, leading to acidification (i.e., SO_4^{2-} and NO_3^-) and/or basification (i.e., NH_4^+, Mg^{2+}, K^+ and Ca^{2+}) together with the CO_2 dissolution from the gas phase. The pH of the cloud samples does not vary a lot, with values ranging from 4.7 to 5.5. Finally, trace metals have been quantified and present very low concentrations. Mg and Zn, which have natural origins like

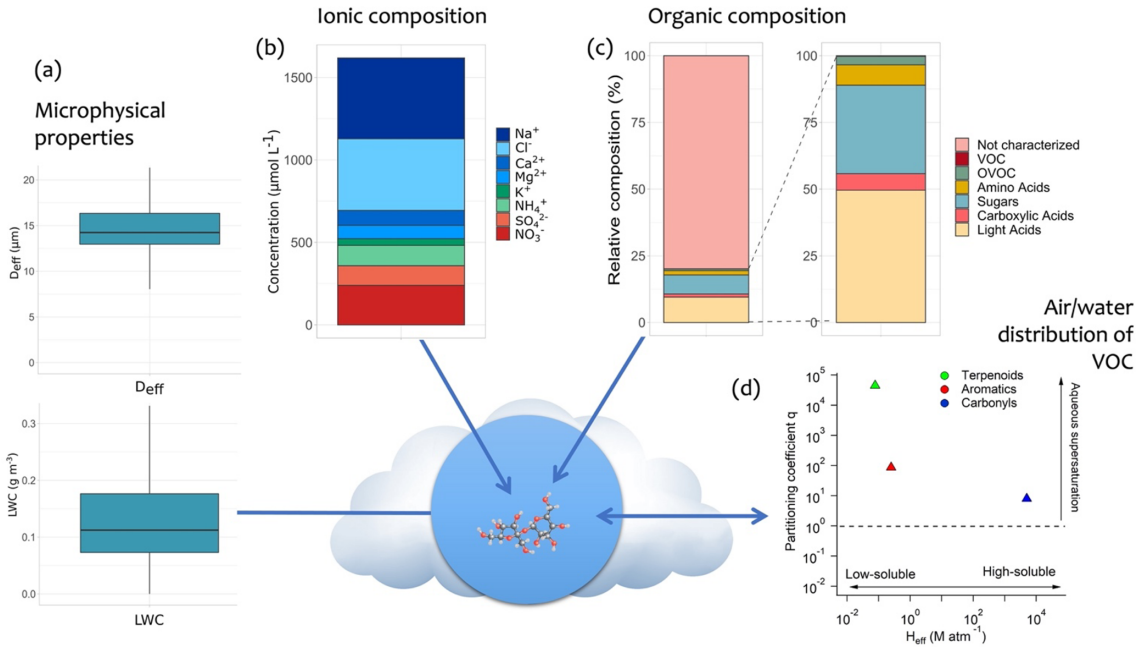

Figure 9. Summary of the main results of the cloud water chemical characterization: **(a)** microphysical properties (LWC and Deff), **(b)** concentration of the main inorganic ions, **(c)** relative organic composition and **(d)** partitioning coefficient q of VOCs between the gaseous and aqueous phases as a function of the effective Henry's law constant (H_{eff}).

sea salt, present the most important concentrations, followed by Cu, Fe, Mn, Ni, Sr and V. These amounts are in the same range as previous studies performed in marine environments (Fomba et al., 2013, 2020) or are influenced by marine emissions (Bianco et al., 2017). Iron speciation has been evaluated with an Fe(II) / Fe(II) + Fe(III) ratio equal to 52 ± 22 %. This suggests an efficient conversion of Fe(III) to Fe(II) and possible complexation of Fe(III) with organics, leading to its stabilization in this redox form. Nonetheless, the effect of iron on the oxidative budget is expected to be low due to low Fe concentrations ($0.88 \pm 0.19\,\mu\mathrm{mol\,L^{-1}}$ on average).

Dissolved organic compounds have also been intensively investigated during the campaign. The average concentration of dissolved organic carbon (DOC) is equal to $25.5 \pm 19.2\,\mathrm{mg\,C\,L^{-1}}$, which is much higher than values reported for cloud waters sampled in marine environments such as in the South Pacific Ocean (Benedict et al., 2012), Puerto Rico (Reyes-Rodriguez et al., 2009), southern Asia (Stahl et al., 2021) or the Puy de Dôme station for clouds under marine influence (Deguillaume et al., 2014). Like for inorganics, this indicates additional inputs of DOC other than sea-related ones. Among the quantified compounds, organic acids and sugars contribute on average a significant fraction of the DOC (around 18 %) (Fig. 9c). Light carboxylic acids, such as formic and acetic acids, are dominant compounds and present concentrations higher than those observed in marine environments. Results indicate that their concentration in the aqueous phase is mainly due to mass transfer from the gas phase, in which they are emitted by anthropogenic and biogenic primary sources. The most concentrated dicarboxylic acids are lactic and oxalic acids, resulting from the reactivity in the aqueous phase or from the dissolution of the CCN. Reported concentrations of dicarboxylic acids are rather low compared to other sites, probably because clouds freshly form over the mountain slope, which does not allow their efficient production by aqueous reactivity. Sugars are also ubiquitous in all our samples and derive mainly from the water-soluble fraction of the CCN. The aqueous concentration of sugars is equal on average to $22.2 \pm 15.4\,\mu\mathrm{mol\,L^{-1}}$, and the calculated atmospheric concentration ($121.3 \pm 69.6\,\mathrm{ng\,m^{-3}}$) is important compared to previous aerosol studies (Verma et al., 2018; Zhu et al., 2015). This can be explained by the importance of biogenic emissions at Réunion but potentially also by the production by microorganisms in cloud water. Identically to sugars, amino acids are issued from biogenic production. They have been measured with total concentrations of free amino acids (TCAAs) varying from 0.8 to $21.1\,\mu\mathrm{mol\,L^{-1}}$ (average $4.6 \pm 5.5\,\mu\mathrm{mol\,L^{-1}}$), representing 1.6 % of the DOC on average. These values are higher than those reported at a marine site in Cabo Verde by Triesch et al. (2021) and much higher than those measured at the Puy de Dôme station (Renard et al., 2022). This fact can be explained by the surrounding potentially important sources (sea surface but also vegetation). Among the 15 amino acids detected, serine, alanine and glycine are dominant; a plausible explanation is related to their high atmospheric lifetimes due to low reactivity with hydroxyl radicals and their preponderance in biological matrices. Finally, carbonyls (OVOCs) and

low-solubility VOCs have been investigated. The average concentration of carbonyls is $3.5 \pm 1.7\,\mu mol\,L^{-1}$ (on average 42.0 % of formaldehyde, 14.2 % of hydroxyacetaldehyde, 11.3 % of acetaldehyde, 10.4 % of acetone, 9.8 % of glyoxal, 6.9 % of hydroxyacetone and 5.3 % of methyl glyoxal), representing 1 % of the DOC on average. This global amount is rather low compared to other studies, and the formaldehyde-to-acetaldehyde ratio suggests a contribution of vegetation emissions. Terpenoids (α-pinene, β-pinene and limonene) and isoprene have been detected together with primary aromatics (benzene, toluene, ethylbenzene and xylenes) in the $nmol\,L^{-1}$ range, contributing 0.35 % of the DOC. Despite their low concentrations, they are of interest since they are tracers of emissions and allow for evaluation of air–droplet partitioning (see below).

The contribution of the organic compounds targeted in this project represents around 20 % on average of the DOC concentration, reaching up to 35 % for one specific cloud. Recently, cloud organic matter was assessed by high-resolution mass spectrometry using the FT-ICR MS instrument (Cook et al., 2017; Bianco et al., 2018; Sun et al., 2021). Thousands of molecular formulae could be potentially detected in cloud water, and their presence and concentration are often related to the influence of primary sources and atmospheric processing. The analysis by FT-ICR MS requires at least 50 mL of cloud water, which is thereafter pre-concentrated and desalted by solid-phase extraction. Three samples (R8, R9 and R10B) presenting enough volume have been analyzed with this instrument equipped with an electrospray ionization (ESI) source set in negative ionization mode. The assigned molecular formula retrieved by high-resolution mass spectra does not enable the attribution of a structural formula. Nevertheless, based on the elemental composition, considering the number of carbon, oxygen, nitrogen, hydrogen and sulfur atoms, the molecular formula can be classified into compounds of biogenic or anthropogenic origin, such as lipids, carbohydrates, proteins or unsaturated hydrocarbons and condensed aromatics, respectively. This analysis offers the possibility of getting information on the DOC fraction not characterized by previously presented targeted analysis. Results of this DOC characterization of cloud water collected at Réunion are reported and compared to the chemical composition of samples collected at the Puy de Dôme station (France) in Pailler et al. (2023a) and compared to the chemical composition of samples collected at the Puy de Dôme station (France). Thousands of molecules have been detected, with a significant fraction (50 %) composed of reduced compounds belonging to lipids probably linked to primary emissions from vegetation, the marine surface and urban areas.

In addition to the chemical characterization, specific attention has been paid to the distribution of VOCs between the gas and aqueous phases in the cloudy atmosphere and to the environmental variability of the chemical composition. For OVOCs, a small deviation from Henry's law equilibrium has been observed. However, high supersaturation in the aqueous phase is measured for low-solubility biogenic and anthropogenic compounds as previously described in van Pinxteren et al. (2005) and Wang et al. (2020) (Fig. 9d). Possible explanations are interactions of these compounds with dissolved or colloidal matter or adsorption at the air–water interface.

A statistical analysis has been performed combining cloud chemical data with back-trajectory calculations derived from Meso-CAT associated with the Corine 2018 land cover database. This work shows that air mass origins and microphysical variables cannot explain the evolutions observed in cloud chemical composition. This reveals the complexity of interconnected processes occurring on the mountain slopes (i.e., emission sources, multiphase transfer and chemical processing in clouds).

3.6 Biological measurements: cloud water and aerosols

The diversity of culturable bacteria from clouds collected at PO-4 during this campaign is reported, along with others, in Charpentier et al. (2024). These included 105 distinct strains, most of which (58 %) were affiliated with Proteobacteria (39 % Gammaproteobacteria, 12 % Alphaproteobacteria and 7 % Betaproteobacteria), followed by Actinobacteria (34 %) and Firmicutes (7 %). The most represented species comprised *Stenotrophomonas*, *Pseudomonas* and *Acinetobacter* in Gammaproteobacteria, *Microbacterium* and *Curtobacterium* in Actinobacteria, *Bosea* and *Sphingomonas* in Alphaproteobacteria, as well as *Bacillus* in Firmicutes. This is a common pattern for viable bacteria in atmospheric samples (e.g., Vaïtilingom et al., 2012).

Bacteria diversity profiling by high-throughput sequencing from 74 aerosol samples collected at PF-1 and Maïdo indicated the presence of 8437 $OTU_{0.03}$ (operational taxonomy units clustered at 97 % sequence similarity, i.e., the $\sim$ prokaryotic species level; see Amato et al. (2017) for details) in total, of which 6935 were affiliated at > 95 % identity to know sequences in databases. The vast majority of these (99.6 %) were bacteria, the rest being attributed to Archaea. As for culturable bacteria from clouds, the phylum Proteobacteria dominated (29.3 % of the sequences), followed by Firmicutes, Actinobacteria and Bacteroidetes, each represented by ~ 16 % of the sequences. Among others, Cyanobacteria, Planctomycetes and Acidobacteria notably each contributed 3 % to 4 % of the sequences. This composition is consistent with airborne bacteria in other places of the planet using similar methods (e.g., Amato et al., 2017; Péguilhan et al., 2021).

4 Discussion

Online measurements of VOCs during the campaign show, as expected, the presence of BVOCs dominated by isoprene along the slope of the Maïdo and at the observatory during the daytime. The effect of cloud on mixing ratios of isoprene and its oxidation products is clear, looking at their diurnal

variation for cloudy days (see Fig. 4 in Rocco et al., 2022). It is well known that clouds induce less efficient emission of isoprene due to the decrease in solar radiation and temperature (e.g., Guenther et al., 1993), but the scavenging of isoprene and its oxidation products in cloud droplets could also contribute to their decrease. Dominutti et al. (2022b) showed that isoprene has been detected in almost all the samplings of cloud water during the campaign (at a concentration of about a few dozen nanomol per liter). Furthermore, despite BTEX being poorly soluble in water, BTEXs were detected in all the cloud water samples with a mean concentration of 4.2 nmol L^{-1}, showing that clouds act as a sink for aromatic compounds. However, even if the level of oxidation products from isoprene decreases from PF-1 to MO-5 for days where both sites are dynamically connected, VOC measurements do not allow determination of the importance of the photochemistry versus the dilution and deposition on the air mass composition sampled at MO-5 (Rocco et al., 2022).

The analysis of PM_{10} filters shows that, even if the concentration of OM is lower at MO-5 than at PF-1, the concentration of dicarboxylic acids is highest at MO-5, especially in the second part of the campaign, where oxalate is detected only at MO-5 (Fig. 8a) and which was cloudier. The PMF analysis of the submicron aerosols at MO-5 shows that the more oxidized organic fraction of aerosols (MOOAs) is the dominant part of the organic aerosol, and its contribution increases during the second part of the campaign (Dominutti et al., 2022a). These results seem to underline the possible effect of cloud processing on the organic composition of particles sampled at MO-5. An analysis combining observations of PM_{10} compositions, aerosol size distributions, contributions of PMF factors and results of simulated clouds along the slope from the Meso-NH model highlights the role of cloud processing in aerosols sampled at MO-5 (Dominutti et al., 2022a). Observations showed a shift to a larger diameter of the aerosol size distribution (15 % for the Aitken and accumulation modes) and an increase of 10 % of the contributions of sulfate and MOOAs in the chemical composition of submicron particles when cloud processing occurs during the daytime (Dominutti et al., 2022a).

The database from the BIO-MAÏDO campaign is a unique opportunity to better understand the contribution of multiphase atmospheric chemistry to SOA formation. However, deep analysis of the database does not allow quantification of this contribution, even if it shows clear evidence of cloud processing in the OM composition of particles sampled at MO-5. Simulations with the explicit cloud chemistry model CLEPS are ongoing to investigate organic matter processing by clouds. A case study has been selected for this simulation, and 28 March 2019 was chosen for several reasons: the amount of cloud water sampling was sufficient to allow deep chemical composition analysis (Dominutti et al., 2022b), the observed cloud for that day is typical of a cloud forming on the slope at the end of the morning and evaporating before arriving at the MO-5 (see Sect. 3.2), the operation of the instruments was almost complete, and there is evidence for sampling of air masses advected along the slope at MO-5 (Rocco et al., 2022). The CLEPS simulation is driven by meteorological and cloud microphysical parameters extracted from a trajectory coming from the Meso-NH's smallest domain (100 m horizontal resolution) for this specific cloud event. The contribution of biodegradation to the cloud processing will be assessed thanks to a recent development in the CLEPS model (Pailler et al., 2023b). Biodegradation rates considered in the model have been determined using microbial strains that have been isolated from the Puy de Dôme station. However, this is not problematic since the comparison of the profiles of the phylum-level distributions of bacteria isolates from clouds at Réunion and at Puy de Dôme shows close similarities (Charpentier et al., 2024). Microorganisms' metabolic activities could be even more efficient at Réunion due to more elevated temperature, and this can be parameterized in the model.

In parallel with this 0D modeling, based on the 3D Meso-NH simulation done for the entire campaign, other Meso-NH simulations were done for the specific period from 28 to 30 March. El Gdachi et al. (2023) combined the size and composition of the observed aerosols to couple them to a two-moment microphysical scheme. This new detailed simulation also uses a very high vertical resolution (1 m near the surface) to accurately represent anabatic and katabatic thermal circulations and the formation of clouds on the topography. The 3D studies combining gas-phase chemistry and a detailed inventory of BVOC sources (100 m) are in progress to study the modes of transport and oxidation of organic secondary aerosol precursors. Estimations of emissions of BVOCs at HM-3 (see Sect. 2.4) are used to calibrate and validate simulated emissions fluxes. Both these high-resolution 3D simulations (10 m horizontal resolution and 1 m vertical resolution near the surface) are able to correctly represent the life cycle of clouds and the main thermal circulations on slopes (anabatic and katabatic) (El Gdachi et al., 2024) as well as the source regions and isoprene oxidation mechanisms. Finally, a specific simulation including gas-phase, aerosol and cloud chemistry with Meso-NH will be performed for the case studied with CLEPS. CLEPS simulation will help to select the dominant chemical pathways in the aqueous phase to be considered and/or added to the Meso-NH chemical mechanism. The 3D modeling allows consideration of the complex effects of dynamics, deposition, emissions and photochemistry on the air mass arriving at MO-5.

5 Conclusion

The BIO-MÄIDO campaign was dedicated to the observation of the effect of cloud on the chemical composition of aerosols and especially the organic part in an environment dominated by natural and biogenic emissions. Maïdo

Observatory, which was inaugurated at the end of 2012, was a unique opportunity to fulfill this objective because of its set of instrumentation (https://www.osureunion.fr/les-stations-dobservation/opar/parametres-mesures/, last access: 20 June 2023) and because of its geographical situation: a tropical environment, quasi-daily cloud formation on the slope down the observatory for a specific part of the year, an isolated island with only reduced local anthropogenic influence and an endemic forest on the slope down the observatory. The strategy of the campaign and the choice of the deployed instrumentation were worked out to get the needed parameters to understand the chemical composition of aerosols sampled at the observatory and the signature of the cloud influence on it. The database from the campaign is original, combining dynamical, microphysical, chemical, biological and particle size parameters (droplets and aerosols).

The study of the mixing boundary layer air masses advected by thermal breezes at MO-5 during the daytime shows two preferred trajectory routes, both corresponding to the return branches of the trade winds associated with the upslope thermal breezes. The first preferred route for air mass trajectories passed through the south, allowing air masses to pass over the forests located between 1000 and 1500 m a.s.l. in the southwest of the island. The route of the second set of trajectories goes up the western flank of the island, also indicating a passage in the marine boundary layer. A detailed analysis based on a high-resolution Meso-NH simulation is made for 28 March. This analysis shows an important formation of clouds on the slope of the Maïdo at the end of the morning associated with the anabatic thermal breeze added with the trade wind return loop. These clouds evaporate before arriving at MO-5, indicating that aerosol particles measured at MO-5 can be thought of as having undergone cloud processing during its transport on the slope.

The analysis of VOC measurements shows the highest mixing ratio of BTEX, isoprene and terpenes at PF-1. However, OVOCs are highest at HM-3 and are the highest contributor of the VOC mixing ratio at MO-5. The diminution of BTEX from PF-1 to HM-3 to MO-5 is a signature of the decrease in the influence of anthropogenic emissions along the slope to the Maïdo, as expected. The study of the chemical composition of particles at PF-1 and MO-5 during the daytime shows the presence of more oxidized organic aerosol at MO-5 and a higher concentration of oxalic acids at MO-5 than at PF-1. Both results indicate the presence of photochemically aged aerosols at MO-5, potentially impacted by cloud processing depending on the day and the trajectories of air masses arriving at MO-5. The analysis of the cloud chemical composition allows a thorough identification of organic compounds in cloud water. This in-depth analysis of organic compounds in cloud water allowed us to characterize around 20 % on average of the dissolved organic compounds.

These results, obtained from analysis of the BIO-MAÏDO campaign database, must be completed by numerical modeling to meet the three main objectives of the BIO-MAÏDO project, i.e., to understand which are the main formation pathways of SOA in a humid tropical atmosphere (gaseous phase versus aqueous phase); to improve multiphase processes leading to SOA formation in a 3D model; and to examine whether the presence of bacteria in the aqueous phase could contribute to SOA formation. To assess these objectives, simulations with the explicit cloud chemistry CLEPS model and the 3D Meso-NH are underway. Results from CLEPS will help to develop more complete chemical mechanisms for the 3D Meso-NH model to understand the role of biogenic influence on SOA formation in cloud water in a tropical environment.

The BIO-MAÏDO project focuses on the effect of cloud on SOA formation in a tropical environment under biogenic influence dominated by isoprene emissions. During recent years, several studies using FT-ICR MS revealed that CHON formulas had a high contribution to dissolved organic carbon in cloud water sampling in Colorado, USA (Zhao et al., 2013), New York, USA (Cook et al., 2027), the center of France (Bianco et al., 2018, 2019) and southern China (Sun et al., 2021; Guo et al., 2023). Similar analysis is underway of three cloud samplings of the BIO-MAÏDO campaign. CHON compounds can have precursors from biomass burning (BB) and anthropogenic and biogenic emissions. For instance, Paglione et al. (2020) observed SOA formation by aqueous-phase processing of wood combustion during wintertime in the Po Valley area under the influence of fog and low-level clouds. Moreover, part of these compounds present in cloud water can lead to the formation of potentially toxic and harmful aqueous SOA as shown by Witkowski et al. (2022) in the lab, who studied the aqueous oxidation by OH of nitrophenols. These recent developments in the analysis of the composition of cloud water and the formation of SOA through aqueous-phase chemistry show a need to include more complete chemical mechanisms to understand the role of anthropogenic and BB influence on SOA formation in cloud and fog water, which is still not well understood. This can be investigated using available kinetics data and structure activity relationships for such chemical development (Hoffmann et al., 2018; González-Sánchez et al., 2021; Li et al., 2023). Future projects involving field campaigns following the BIO-MAÏDO methodology should be developed to assess a more complete understanding of the influence of cloud chemistry on the formation of SOA.

Code and data availability. The data from the BIO-MAÏDO campaign can be accessed via https://doi.org/10.25326/502 (Leriche, 2023). The 3D simulations were produced with the Meso-NH code, which is maintained and updated by LAERO and CNRM and which is freely available for download at http://mesonh.aero.obs-mip.fr/ (LAERO, 2024).

Supplement. The supplement related to this article is available online at: https://doi.org/10.5194/acp-24-4129-2024-supplement.

Author contributions. ML is the principal investigator of the BIO-MAÏDO program and designed the field campaign and prepared the manuscript with contributions from all the authors. PT organized the field campaign, produced and organized the strategy for the Meso-NH simulations, and took part in the analysis of the results shown in the paper. LD led Task 3 of the project on cloud sampling and characterization, wrote and reviewed the paper, and took part in the field campaign. FB co-led Task 1 dedicated to atmospheric dynamic and cloud properties and led the tethered balloon operations and the cloud microphysics instrumentation network. AC was responsible for the VOC measurements, wrote and reviewed the paper related to gaseous atmospheric composition analysis, and took part in the field experiments. AgB co-led Task 2 of the project related to the analysis of physicochemical processes, wrote and reviewed the paper related to gaseous atmospheric composition analysis, and took part in the field experiments. CJ co-led Task 2 of the project related to the analysis of physicochemical processes, led the HM-3 station, and participated in the field experiment and the data treatment and analysis for this site. VD organized the field campaign and analyzed the lidar measurements. SH, JLJ and PD supervised the analyses of the offline PM samples, processed these data, and commented on the overall manuscript. MV co-organized and participated in the cloud droplet sampling and was responsible for the culture of bacteria from the cloud samplings at the site. PD supervised the analyses of the offline PM samples and some of the analysis of the cloud samples, processed these data, and commented on the whole manuscript. MaR wrote and reviewed the paper related to gaseous atmospheric composition analysis and took part in the field experiments. CMV was involved in the analysis of the cloud chemistry measurements. SEG was involved in the dynamical analysis of the campaign. MB participated in the cloud sampling during the field campaign. MF and NM participated in the tethered balloon operations. BV operated the FLEXPART-AROME model: this included the design of the automated back-trajectory forecasting system which was operational during the BIO-MAÏDO campaign and provided updated footprints afterwards. CA, NS and BV were responsible for the deployment, operation and VOC database generation of the BIRA-IASB PTR-MS located at MO-5. VG was responsible for the PTR-MS installed in the Atmo-Réunion truck and took part in the field campaign. JMP and MiR participated in collecting the cloud droplets and VOCs and OVOCs at PO-4. EP participated in the HM-3 station installation and the field experiment. EL participated in the field experiment and the HM-3 station disassembly. TB led in situ aerosol measurements at DOS-2. AR, EM and JB participated in the tethered balloon operations. JMM was in charge of the technical support at MO-5 for the instrumentation deployed for the BIO-MÄIDO campaign. GP, CG, CB, JMT and AT were responsible for the Atmo-Réunion truck deployment. EF, JLJ and PD wrote and reviewed the paper related to aerosol and cloud composition analysis. KS was involved in the analysis of the aerosol measurements. AMD was involved in the analysis of the bacteria measurements. PA and MJ isolated and identified the microbial strains and performed the meta-barcoding sequencing. JLB performed the back-trajectory and dynamical analysis. PR, AnB, LD and PD analyzed the cloud samples at the lab. AR was involved in the dynamical analysis of the campaign. GP was involved in the lidar measurements and their analysis. All reviewed the paper.

Competing interests. The contact author has declared that none of the authors has any competing interests.

Disclaimer. Publisher's note: Copernicus Publications remains neutral with regard to jurisdictional claims made in the text, published maps, institutional affiliations, or any other geographical representation in this paper. While Copernicus Publications makes every effort to include appropriate place names, the final responsibility lies with the authors.

Acknowledgements. The authors thank AERIS (French national pole for atmospheric services and data: https://www.aeris-data.fr/, last access: 20 June 2023) for its support on data storage. The French Meteorological Office (DIROI/Météo-France) also helped the management of the campaign by providing day-by-day meteorological forecasting. The authors gratefully acknowledge the CNRS-INSU (Institut National des Sciences de l'Univers) for supporting the measurements performed at MO-5, which is part of the SI-OPAR (Observatoire de Physique de l'Atmosphère à La Réunion), and those within the long-term monitoring aerosol program SNO-CLAP (Climate relevant Aerosol Properties from near-surface observations), both of which are components of the ACTRIS French research infrastructure and whose data are hosted at the AERIS data center. The authors thank the staff of UAR3365 in charge of reception at MO-5. Meso-NH simulations were done on the Météo-France supercomputer. The map data used in Fig. 1 are from OpenStreetMap (https://www.openstreetmap.org/copyright/en, last access: 21 March 2024). Saint-Paul City Hall is thanked for its support and its authorization to install scientific instrumentation on the HM-3 site. All the participants in the campaign wish to thank Doudou for his hospitality at the DOS-2 site.

Financial support. The BIO-MAÏDO project was funded by the Agence Nationale de la Recherche (grant no. ANR-18-CE01-0013). The deployment of the BIRA-IASB PTR-MS at Maïdo Observatory was supported by the Belgian Federal Science Policy Office (grant no. BR/175/A2/OCTAVE) with additional funding from Horizon 2020 (ACTRIS-2, grant no. 654109).

Review statement. This paper was edited by Alex Huffman and reviewed by two anonymous referees.

References

Amato, P., Joly, M., Besaury, L., Oudart, A., Taib, N., Moné, A. I., Deguillaume, L., Delort, A.-M., and Debroas, D.: Active microorganisms thrive among extremely diverse communities in cloud water, PLoS ONE, 12, e0182869, https://doi.org/10.1371/journal.pone.0182869, 2017.

Amelynck, C., Schoon, N., and Verreyken, B.: Long-term in situ (O) VOCs measurements at the Maïdo observatory (Reunion Island), Royal Belgian Institute for Space Aeronomy (BIRA-IASB) [data set], https://doi.org/10.18758/71021061, 2021.

Baray, J.-L., Courcoux, Y., Keckhut, P., Portafaix, T., Tulet, P., Cammas, J.-P., Hauchecorne, A., Godin Beekmann, S., De Mazière, M., Hermans, C., Desmet, F., Sellegri, K., Colomb, A., Ramonet, M., Sciare, J., Vuillemin, C., Hoareau, C., Dionisi, D., Duflot, V., Vérèmes, H., Porteneuve, J., Gabarrot, F., Gaudo, T., Metzger, J.-M., Payen, G., Leclair de Bellevue, J., Barthe, C., Posny, F., Ricaud, P., Abchiche, A., and Delmas, R.: Maïdo observatory: a new high-altitude station facility at Reunion Island (21° S, 55° E) for long-term atmospheric remote sensing and in situ measurements, Atmos. Meas. Tech., 6, 2865–2877, https://doi.org/10.5194/amt-6-2865-2013, 2013.

Baray, J.-L., Deguillaume, L., Colomb, A., Sellegri, K., Freney, E., Rose, C., Van Baelen, J., Pichon, J.-M., Picard, D., Fréville, P., Bouvier, L., Ribeiro, M., Amato, P., Banson, S., Bianco, A., Borbon, A., Bourcier, L., Bras, Y., Brigante, M., Cacault, P., Chauvigné, A., Charbouillot, T., Chaumerliac, N., Delort, A.-M., Delmotte, M., Dupuy, R., Farah, A., Febvre, G., Flossmann, A., Gourbeyre, C., Hervier, C., Hervo, M., Huret, N., Joly, M., Kazan, V., Lopez, M., Mailhot, G., Marinoni, A., Masson, O., Montoux, N., Parazols, M., Peyrin, F., Pointin, Y., Ramonet, M., Rocco, M., Sancelme, M., Sauvage, S., Schmidt, M., Tison, E., Vaïtilingom, M., Villani, P., Wang, M., Yver-Kwok, C., and Laj, P.: Cézeaux-Aulnat-Opme-Puy De Dôme: a multi-site for the long-term survey of the tropospheric composition and climate change, Atmos. Meas. Tech., 13, 3413–3445, https://doi.org/10.5194/amt-13-3413-2020, 2020.

Bates, K. H., Jacob, D. J., Wang, S., Hornbrook, R. S., Apel, E. C., Kim, M. J., Millet, D. B., Wells, K. C., Chen, X., Brewer, J. F., Ray, E. A., Commane, R., Diskin, G. S., and Wofsy, S. C.: The Global Budget of Atmospheric Methanol: New Constraints on Secondary, Oceanic, and Terrestrial Sources, J. Geophys. Res.-Atmos., 126, e2020JD033439, https://doi.org/10.1029/2020JD033439, 2021.

Bauer, H., Schueller, E., Weinke, G., Berger, A., Hitzenberger, R., Marr, I. L., and Puxbaum, H.: Significant contributions of fungal spores to the organic carbon and to the aerosol mass balance of the urban atmospheric aerosol, Atmos. Environ., 42, 5542–5549, https://doi.org/10.1016/j.atmosenv.2008.03.019, 2008.

Benedict, K. B., Lee, T., and Collett, J. L.: Cloud water composition over the southeastern Pacific Ocean during the VOCsALS regional experiment, Atmos. Environ., 46, 104–114, https://doi.org/10.1016/j.atmosenv.2011.10.029, 2012.

Bianco, A., Vaïtilingom, M., Bridoux, M., Chaumerliac, N., Pichon, J.-M., Piro, J.-L., and Deguillaume, L.: Trace metals in cloud water sampled at the Puy de Dôme station, Atmosphere, 8, 225, https://doi.org/10.3390/atmos8110225, 2017.

Bianco, A., Deguillaume, L., Vaitilingom, M., Nicol, E., Baray, J. L., Chaumerliac, N., and Bridoux, M.: Molecular characterization of cloud water samples collected at the Puy de Dome (France) by Fourier Transform Ion Cyclotron Resonance Mass Spectrometry, Environ. Sci. Technol., 52, 10275–10285, https://doi.org/10.1021/acs.est.8b01964, 2018.

Bianco, A., Riva, M., Baray, J.-L., Ribeiro, M., Chaumerliac, N., George, C., Bridoux, M., and Deguillaume, L.: Chemical characterization of cloudwater collected at Puy de Dôme by FT-ICR MS reveals the presence of SOA components, ACS Earth Space Chem., 3, 2076–2087, https://doi.org/10.1021/acsearthspacechem.9b00153, 2019.

Borlaza, L. J. S., Weber, S., Uzu, G., Jacob, V., Cañete, T., Micallef, S., Trébuchon, C., Slama, R., Favez, O., and Jaffrezo, J.-L.: Disparities in particulate matter (PM_{10}) origins and oxidative potential at a city scale (Grenoble, France) – Part 1: Source apportionment at three neighbouring sites, Atmos. Chem. Phys., 21, 5415–5437, https://doi.org/10.5194/acp-21-5415-2021, 2021.

Boucher, O., Randall, D., Artaxo, P., Bretherton, C., Feingold, G., Forster, P., Kerminen, V.-M., Kondo, Y., Liao, H., Lohmann, U., Rasch, P., Satheesh, S. K., Sherwood, S., Stevens, B., and Zhang, X. Y.: Clouds and Aerosols, in: Climate Change 2013: The Physical Science Basis. Contribution of Working Group I to the Fifth Assessment Report of the Intergovernmental Panel on Climate Change, edited by: Stocker, T. F., Qin, D., Plattner, G.-K., Tignor, M., Allen, S. K., Boschung, J., Nauels, A., Xia, Y., Bex, V., and Midgley, P. M., Cambridge University Press, Cambridge, United Kingdom and New York, NY, USA, ISBN: 978-1-107-05799-1, 2013.

Brito, J., Freney, E., Dominutti, P., Borbon, A., Haslett, S. L., Batenburg, A. M., Colomb, A., Dupuy, R., Denjean, C., Burnet, F., Bourriane, T., Deroubaix, A., Sellegri, K., Borrmann, S., Coe, H., Flamant, C., Knippertz, P., and Schwarzenboeck, A.: Assessing the role of anthropogenic and biogenic sources on PM_1 over southern West Africa using aircraft measurements, Atmos. Chem. Phys., 18, 757–772, https://doi.org/10.5194/acp-18-757-2018, 2018.

Canonaco, F., Crippa, M., Slowik, J. G., Baltensperger, U., and Prévôt, A. S. H.: SoFi, an IGOR-based interface for the efficient use of the generalized multilinear engine (ME-2) for the source apportionment: ME-2 application to aerosol mass spectrometer data, Atmos. Meas. Tech., 6, 3649–3661, https://doi.org/10.5194/amt-6-3649-2013, 2013.

Caporaso, J. G., Lauber, C. L., Walters, W. A., Berg-Lyons, D., Huntley, J., Fierer, N., Owens, S. M., Betley, J., Fraser, L., Bauer, M., Gormley, N., Gilbert, J. A., Smith, G., and Knight, R.: Ultra-high-throughput microbial community analysis on the Illumina HiSeq and MiSeq platforms, ISME J., 6, 1621–1624, https://doi.org/10.1038/ismej.2012.8, 2012.

Carlton, A. G., Turpin, B. J., Altieri, K. E., Seitzinger, S., Reff, A., Lim, H.-J., and Ervens, B.: Atmospheric oxalic acid and SOA production from glyoxal: Results of aqueous photooxidation experiments, Atmos. Environ., 41, 7588–7602, 2007.

Cavalli, F., Viana, M., Yttri, K. E., Genberg, J., and Putaud, J.-P.: Toward a standardised thermal-optical protocol for measuring atmospheric organic and elemental carbon: the EUSAAR protocol, Atmos. Meas. Tech., 3, 79–89, https://doi.org/10.5194/amt-3-79-2010, 2010.

Charpentier, T., Joly, M., Judon, C., Sancelme, M., Abrantes, M., Vaïtilingom, M., Ghaffar, C., Brissy, M., Leriche, M., Delort, A.-M., Deguillaume, L., and Amato, P.: Culturable bacteria in clouds at Réunion, tropical island, Aerobiologica, 2024.

Cheng, C., Wang, G., Zhou, B., Meng, J., Li, J., Cao, J., and Xiao, S.: Comparison of dicarboxylic acids and related compounds in aerosol samples collected in Xi'an, China during haze and clean periods, Atmos. Environ., 81, 443–449, https://doi.org/10.1016/j.atmosenv.2013.09.013, 2013.

Cook, R. D., Lin, Y.-H., Peng, Z., Boone, E., Chu, R. K., Dukett, J. E., Gunsch, M. J., Zhang, W., Tolic, N., Laskin, A., and Pratt, K. A.: Biogenic, urban, and wildfire influences on the molecular composition of dissolved organic compounds in cloud water, Atmos. Chem. Phys., 17, 15167–15180, https://doi.org/10.5194/acp-17-15167-2017, 2017.

Deguillaume, L., Charbouillot, T., Joly, M., Vaïtilingom, M., Parazols, M., Marinoni, A., Amato, P., Delort, A.-M., Vinatier, V., Flossmann, A., Chaumerliac, N., Pichon, J. M., Houdier, S., Laj, P., Sellegri, K., Colomb, A., Brigante, M., and Mailhot, G.: Classification of clouds sampled at the puy de Dôme (France) based on 10 yr of monitoring of their physicochemical properties, Atmos. Chem. Phys., 14, 1485–1506, https://doi.org/10.5194/acp-14-1485-2014, 2014.

Dominutti, P. A., Chevassus, E., Baray, J.-L., Jaffrezo, J.-L., Borbon, A., Colomb, A. Deguillaume, L., El Gdachi, S., Houdier, S., Leriche, M., Metzger, J.-M., Rocco, M., Tulet, P., Sellegri, K., and Freney, E.: Evaluation of sources, precursors, and processing of aerosols at a high-altitude tropical site, ACS Earth Space Chem., 6, 2412–2431, https://doi.org/10.1021/acsearthspacechem.2c00149, 2022a.

Dominutti, P. A., Renard, P., Vaïtilingom, M., Bianco, A., Baray, J.-L., Borbon, A., Bourianne, T., Burnet, F., Colomb, A., Delort, A.-M., Duflot, V., Houdier, S., Jaffrezo, J.-L., Joly, M., Leremboure, M., Metzger, J.-M., Pichon, J.-M., Ribeiro, M., Rocco, M., Tulet, P., Vella, A., Leriche, M., and Deguillaume, L.: Insights into tropical cloud chemistry in Réunion (Indian Ocean): results from the BIO-MAÏDO campaign, Atmos. Chem. Phys., 22, 505–533, https://doi.org/10.5194/acp-22-505-2022, 2022b.

Duflot, V., Tulet, P., Flores, O., Barthe, C., Colomb, A., Deguillaume, L., Vaïtilingom, M., Perring, A., Huffman, A., Hernandez, M. T., Sellegri, K., Robinson, E., O'Connor, D. J., Gomez, O. M., Burnet, F., Bourrianne, T., Strasberg, D., Rocco, M., Bertram, A. K., Chazette, P., Totems, J., Fournel, J., Stamenoff, P., Metzger, J.-M., Chabasset, M., Rousseau, C., Bourrianne, E., Sancelme, M., Delort, A.-M., Wegener, R. E., Chou, C., and Elizondo, P.: Preliminary results from the FARCE 2015 campaign: multidisciplinary study of the forest–gas–aerosol–cloud system on the tropical island of La Réunion, Atmos. Chem. Phys., 19, 10591–10618, https://doi.org/10.5194/acp-19-10591-2019, 2019.

Ervens, B.: Modeling the Processing of Aerosol and Trace Gases in Clouds and Fogs, Chem. Rev., 115, 4157–4198, https://doi.org/10.1021/cr5005887, 2015.

Ervens, B. and Amato, P.: The global impact of bacterial processes on carbon mass, Atmos. Chem. Phys., 20, 1777–1794, https://doi.org/10.5194/acp-20-1777-2020, 2020.

Ervens, B., Turpin, B. J., and Weber, R. J.: Secondary organic aerosol formation in cloud droplets and aqueous particles (aqSOA): a review of laboratory, field and model studies, Atmos. Chem. Phys., 11, 11069–11102, https://doi.org/10.5194/acp-11-11069-2011, 2011.

Escudié, F., Auer, L., Bernard, M., Mariadassou, M., Cauquil, L., Vidal, K., Maman, S., Hernandez-Raquet, G., Combes, S., and Pascal, G.: FROGS: Find, Rapidly, OTUs with Galaxy Solution, Bioinformatics, 34, 1287–1294, https://doi.org/10.1093/bioinformatics/btx791, 2018.

European Environment Agency: CORINE Land Cover 2018 (raster 100 m), Europe, 6-yearly – version 2020_20u1, May 2020, European Union's Copernicus Land Monitoring Service [dataset], https://doi.org/10.2909/960998c1-1870-4e82-8051-6485205ebbac, 2020.

Fathalli, M., Lac, C., Burnet, F., and Vié, B.: Formation of fog due to stratus lowering: an observational and modelling case study, Q. J. Roy. Meteor. Soc., 148, 2299–2324, https://doi.org/10.1002/qj.4304, 2022.

Fomba, K. W., Müller, K., van Pinxteren, D., and Herrmann, H.: Aerosol size-resolved trace metal composition in remote northern tropical Atlantic marine environment: case study Cape Verde islands, Atmos. Chem. Phys., 13, 4801–4814, https://doi.org/10.5194/acp-13-4801-2013, 2013.

Fomba, K. W., Deabji, N., Barcha, S. E. I., Ouchen, I., Elbaramoussi, E. M., El Moursli, R. C., Harnafi, M., El Hajjaji, S., Mellouki, A., and Herrmann, H.: Application of TXRF in monitoring trace metals in particulate matter and cloud water, Atmos. Meas. Tech., 13, 4773–4790, https://doi.org/10.5194/amt-13-4773-2020, 2020.

Gioda, A., Mayol-Bracero, O. L., Scatena, F. N., Weathers, K. C., Mateus, V. L., and McDowell, W. H.: Chemical constituents in clouds and rainwater in the Puerto Rican rainforest: Potential sources and seasonal drivers, Atmos. Environ., 68, 208–220, https://doi.org/10.1016/j.atmosenv.2012.11.017, 2013.

Foucart, B., Sellegri, K., Tulet, P., Rose, C., Metzger, J.-M., and Picard, D.: High occurrence of new particle formation events at the Maïdo high-altitude observatory (2150 m), Réunion (Indian Ocean), Atmos. Chem. Phys., 18, 9243–9261, https://doi.org/10.5194/acp-18-9243-2018, 2018.

Golly, B., Waked, A., Weber, S., Samake, A., Jacob, V., Conil, S., Rangognio, J., Chrétien, E., Vagnot, M.-P., Robic, P.-Y., Besombes, J.-L., and Jaffrezo, J.-L.: Organic markers and OC source apportionment for seasonal variations of $PM_{2.5}$ at 5 rural sites in France, Atmos. Environ., 198, 142–157, https://doi.org/10.1016/j.atmosenv.2018.10.027, 2019.

González-Sánchez, J. M., Brun, N., Wu, J., Morin, J., Temime-Roussel, B., Ravier, S., Mouchel-Vallon, C., Clément, J.-L., and Monod, A.: On the importance of atmospheric loss of organic nitrates by aqueous-phase •OH oxidation, Atmos. Chem. Phys., 21, 4915–4937, https://doi.org/10.5194/acp-21-4915-2021, 2021.

Guenther, A. B., Zimmerman, P. R., Harley, P. C., Monson, R. K., and Fall, R.: Isoprene and Monoterpene Emission Rate Variability – Model Evaluations and Sensitivity Analyses, J. Geophys. Res.-Atmos., 98, 12609–12617, 1993.

Guenther, A. B., Jiang, X., Heald, C. L., Sakulyanontvittaya, T., Duhl, T., Emmons, L. K., and Wang, X.: The Model of Emissions of Gases and Aerosols from Nature version 2.1 (MEGAN2.1): an extended and updated framework for modeling biogenic emissions, Geosci. Model Dev., 5, 1471–1492, https://doi.org/10.5194/gmd-5-1471-2012, 2012.

Guilpart, E., Vimeux, F., Evan, S., Brioude, J., Metzger, J.-M., Barthe, C., Risi, C., and Cattani, O.: The isotopic composition of near-surface water vapor at the Maïdo observatory (Reunion Island, southwestern Indian Ocean) documents the controls of the humidity of the subtropical troposphere, J. Geophys. Res.-Atmos., 122, 9628–9650, https://doi.org/10.1002/2017JD026791, 2017.

Guo, Z., Sun, W., Hu, X., Lin, J., Fu, Y., Peng, X., Jiang, B., Liao, Y., Zhang, G., Wang, X., Peng, P., and Bi, X.: Molecular characteristics and compositions affecting light absorption features of cloud water revealed by Fourier transform ion cyclotron

resonance mass spectrometry, Atmos. Environ., 295, 119565, https://doi.org/10.1016/j.atmosenv.2022.119565, 2023.

Heald, C. L., Coe, H., Jimenez, J. L., Weber, R. J., Bahreini, R., Middlebrook, A. M., Russell, L. M., Jolleys, M., Fu, T.-M., Allan, J. D., Bower, K. N., Capes, G., Crosier, J., Morgan, W. T., Robinson, N. H., Williams, P. I., Cubison, M. J., DeCarlo, P. F., and Dunlea, E. J.: Exploring the vertical profile of atmospheric organic aerosol: comparing 17 aircraft field campaigns with a global model, Atmos. Chem. Phys., 11, 12673–12696, https://doi.org/10.5194/acp-11-12673-2011, 2011.

Jaffrezo, J.-L., Aymoz, G., Delaval, C., and Cozic, J.: Seasonal variations of the water soluble organic carbon mass fraction of aerosol in two valleys of the French Alps, Atmos. Chem. Phys., 5, 2809–2821, https://doi.org/10.5194/acp-5-2809-2005, 2005.

Jathar, S. H., Cappa, C. D., Wexler, A. S., Seinfeld, J. H., and Kleeman, M. J.: Simulating secondary organic aerosol in a regional air quality model using the statistical oxidation model – Part 1: Assessing the influence of constrained multi-generational ageing, Atmos. Chem. Phys., 16, 2309–2322, https://doi.org/10.5194/acp-16-2309-2016, 2016.

Jimenez, J. L., Canagaratna, M. R., Donahue, N. M., Prevot, A. S. H., Zhang, Q., Kroll, J. H., DeCarlo, P. F., Allan, J. D., Coe, H., Ng, N. L., Aiken, A. C., Docherty, K. S., Ulbrich, I. M., Grieshop, A. P., Robinson, A. L., Duplissy, J., Smith, J. D., Wilson, K. R., Lanz, V. A., Hueglin, C., Sun, Y. L., Tian, J., Laaksonen, A., Raatikainen, T., Rautiainen, J., Vaattovaara, P., Ehn, M., Kulmala, M., Tomlinson, J. M., Collins, D. R., Cubison, M. J., E., Dunlea, J., Huffman, J. A., Onasch, T. B., Alfarra, M. R., Williams, P. I., Bower, K., Kondo, Y., Schneider, J., Drewnick, F., Borrmann, S., Weimer, S., Demerjian, K., Salcedo, D., Cottrell, L., Griffin, R., Takami, A., Miyoshi, T., Hatakeyama, S., Shimono, A., Sun, J. Y., Zhang, Y. M., Dzepina, K., Kimmel, J. R., Sueper, D., Jayne, J. T., Herndon, S. C., Trimborn, A. M., Williams, L. R., Wood, E. C., Middlebrook, A. M., Kolb, C. E., Baltensperger, U., and Worsnop, D. R.: Evolution of Organic Aerosols in the Atmosphere, Science, 326, 1525–1529, https://doi.org/10.1126/science.1180353, 2009.

Kawamura, K. and Bikkina, S.: A review of dicarboxylic acids and related compounds in atmospheric aerosols: Molecular distributions, sources and transformation, Atmos. Res., 170, 140–160, https://doi.org/10.1016/j.atmosres.2015.11.018, 2016.

Kawamura, K. and Sakaguchi, F.: Molecular distributions of water soluble dicarboxylic acids in marine aerosols over the Pacific Ocean including tropics, J. Geophys. Res.-Atmos., 104, 3501–3509, https://doi.org/10.1029/1998JD100041, 1999.

Khaled, A., Zhang, M., Amato, P., Delort, A.-M., and Ervens, B.: Biodegradation by bacteria in clouds: an underestimated sink for some organics in the atmospheric multiphase system, Atmos. Chem. Phys., 21, 3123–3141, https://doi.org/10.5194/acp-21-3123-2021, 2021.

Lac, C., Chaboureau, J.-P., Masson, V., Pinty, J.-P., Tulet, P., Escobar, J., Leriche, M., Barthe, C., Aouizerats, B., Augros, C., Aumond, P., Auguste, F., Bechtold, P., Berthet, S., Bielli, S., Bosseur, F., Caumont, O., Cohard, J.-M., Colin, J., Couvreux, F., Cuxart, J., Delautier, G., Dauhut, T., Ducrocq, V., Filippi, J.-B., Gazen, D., Geoffroy, O., Gheusi, F., Honnert, R., Lafore, J.-P., Lebeaupin Brossier, C., Libois, Q., Lunet, T., Mari, C., Maric, T., Mascart, P., Mogé, M., Molinié, G., Nuissier, O., Pantillon, F., Peyrillé, P., Pergaud, J., Perraud, E., Pianezze, J., Redelsperger, J.-L., Ricard, D., Richard, E., Riette, S., Rodier, Q., Schoetter, R., Seyfried, L., Stein, J., Suhre, K., Taufour, M., Thouron, O., Turner, S., Verrelle, A., Vié, B., Visentin, F., Vionnet, V., and Wautelet, P.: Overview of the Meso-NH model version 5.4 and its applications, Geosci. Model Dev., 11, 1929–1969, https://doi.org/10.5194/gmd-11-1929-2018, 2018.

LAERO: Meso-NH source code download, Laboratoire d'Aérologie (LAERO) and Centre National de Recherches Météorologiques (CNRM) [code], http://mesonh.aero.obs-mip.fr/ (last access: 24 March 2024), 2024.

Leriche, M.: BIO-MAIDO, Aeris [data set], https://doi.org/10.25326/502, 2023.

Lesouëf, D., Gheusi, F., Delmas, R., and Escobar, J.: Numerical simulations of local circulations and pollution transport over Reunion Island, Ann. Geophys., 29, 53–69, https://doi.org/10.5194/angeo-29-53-2011, 2011.

Lesouëf, D., Gheusi, F., Chazette, P., Delmas, R., and Sanak, J.: Low Tropospheric Layers Over Reunion Island in Lidar-Derived Observations and a High-Resolution Model, Bound.-Lay. Meteorol., 149, 425–453, https://doi.org/10.1007/s10546-013-9851-9, 2013.

Li, F., Zhou, S., Du, L., Zhao, J., Hang, J., and Wang, X.: Aqueous-phase chemistry of atmospheric phenolic compounds: A critical review of laboratory studies, Sci. Total Environ., 856, 158895, https://doi.org/10.1016/j.scitotenv.2022.158895, 2023.

McNeill, V. F.: Aqueous organic chemistry in the atmosphere: sources and chemical processing of organic aerosols, Environ. Sci. Technol., 49, 1237–1244, https://doi.org/10.1021/es5043707, 2015.

Molina, L., Wittich, R.-M., van Dillewijn, P., and Segura, A.: Plant-Bacteria Interactions for the Elimination of Atmospheric Contaminants in Cities, Agronomy, 11, 493, https://doi.org/10.3390/agronomy11030493, 2021.

Mouchel-Vallon, C., Deguillaume, L., Monod, A., Perroux, H., Rose, C., Ghigo, G., Long, Y., Leriche, M., Aumont, B., Patryl, L., Armand, P., and Chaumerliac, N.: CLEPS 1.0: A new protocol for cloud aqueous phase oxidation of VOC mechanisms, Geosci. Model Dev., 10, 1339–1362, https://doi.org/10.5194/gmd-10-1339-2017, 2017.

Paglione, M., Gilardoni, S., Rinaldi, M., Decesari, S., Zanca, N., Sandrini, S., Giulianelli, L., Bacco, D., Ferrari, S., Poluzzi, V., Scotto, F., Trentini, A., Poulain, L., Herrmann, H., Wiedensohler, A., Canonaco, F., Prévôt, A. S. H., Massoli, P., Carbone, C., Facchini, M. C., and Fuzzi, S.: The impact of biomass burning and aqueous-phase processing on air quality: a multi-year source apportionment study in the Po Valley, Italy, Atmos. Chem. Phys., 20, 1233–1254, https://doi.org/10.5194/acp-20-1233-2020, 2020.

Pai, S. J., Heald, C. L., Pierce, J. R., Farina, S. C., Marais, E. A., Jimenez, J. L., Campuzano-Jost, P., Nault, B. A., Middlebrook, A. M., Coe, H., Shilling, J. E., Bahreini, R., Dingle, J. H., and Vu, K.: An evaluation of global organic aerosol schemes using airborne observations, Atmos. Chem. Phys., 20, 2637–2665, https://doi.org/10.5194/acp-20-2637-2020, 2020.

Pailler, L., Deguillaume, L., Lavanant, H., Schmitz, I., Hubert, M., Nicol, E., Ribeiro, M., Pichon, J.-M., Vaïtilingom, M., Dominutti, P., Burnet, F., Tulet, P., Leriche, M., and Bianco, A.: Molecular composition of clouds: a comparison between samples collected at tropical (Réunion Island, France) and mid-

north (puy de Dôme, France) latitudes, EGUsphere [preprint], https://doi.org/10.5194/egusphere-2023-2706, 2023a.

Pailler, L., Wirgot, N., Joly, M., Renard, P., Mouchel-Vallon, C., Bianco, A., Leriche, M., Sancelme, M., Job, A., Patryl, L., Armand, P., Delort, A.-M., Chaumerliac, N., and Deguillaume, L.: Assessing the efficiency of water-soluble organic compound biodegradation in clouds under various environmental conditions, Environ. Sci.: Atmos., 3, 731–748, https://doi.org/10.1039/D2EA00153E, 2023b.

Péguilhan, R., Besaury, L., Rossi, F., Enault, F., Baray, J.-L., Deguillaume, L., and Amato, P.: Rainfalls sprinkle cloud bacterial diversity while scavenging biomass, FEMS Microbiol. Ecol., 97, fiab144, https://doi.org/10.1093/femsec/fiab144, 2021.

Pisso, I., Sollum, E., Grythe, H., Kristiansen, N. I., Cassiani, M., Eckhardt, S., Arnold, D., Morton, D., Thompson, R. L., Groot Zwaaftink, C. D., Evangeliou, N., Sodemann, H., Haimberger, L., Henne, S., Brunner, D., Burkhart, J. F., Fouilloux, A., Brioude, J., Philipp, A., Seibert, P., and Stohl, A.: The Lagrangian particle dispersion model FLEXPART version 10.4, Geosci. Model Dev., 12, 4955–4997, https://doi.org/10.5194/gmd-12-4955-2019, 2019.

Quast, C., Pruesse, E., Yilmaz, P., Gerken, J., Schweer, T., Yarza, P., Peplies, J., and Glöckner, F. O.: The SILVA ribosomal RNA gene database project: improved data processing and web-based tools, Nucleic Acids Res., 41, D590–D596, https://doi.org/10.1093/nar/gks1219, 2013.

Réchou, A., Flores, O., Jumaux, G., Duflot, V., Bousquet, O., Pouppeville, C., and Bonnardot, F.: Spatio-temporal variability of rainfall in a high tropical island: Patterns and large-scale drivers in Réunion Island, Q, J. Roy, Meteor. Soc., 145, 893–909, https://doi.org/10.1002/qj.3485, 2019.

Renard, P., Siekmann, F., Salque, G., Demelas, C., Coulomb, B., Vassalo, L., Ravier, S., Temime-Roussel, B., Voisin, D., and Monod, A.: Aqueous-phase oligomerization of methyl vinyl ketone through photooxidation – Part 1: Aging processes of oligomers, Atmos. Chem. Phys., 15, 21–35, https://doi.org/10.5194/acp-15-21-2015, 2015.

Renard, P., Brissy, M., Rossi, F., Leremboure, M., Jaber, S., Baray, J.-L., Bianco, A., Delort, A.-M., and Deguillaume, L.: Free amino acid quantification in cloud water at the Puy de Dôme station (France), Atmos. Chem. Phys., 22, 2467–2486, https://doi.org/10.5194/acp-22-2467-2022, 2022.

Reyes-Rodríguez, G. J., Gioda, A., Mayol-Bracero, O. L., and Collett, J.: Organic carbon, total nitrogen, and water-soluble ions in clouds from a tropical montane cloud forest in Puerto Rico, Atmos. Environ., 43, 4171–4177, https://doi.org/10.1016/j.atmosenv.2009.05.049, 2009.

Rocco, M., Colomb, A., Baray, J. L., Amelynck, C., Verreyken, B., Borbon, A., Pichon, J. M., Bouvier, L., Schoon, N., Gros, V., Sarda-Esteve, R., Tulet, P., Metzger, J. M., Duflot, V., Guadagno, C., Peris, G., and Brioude, J.: Analysis of volatile organic compounds during the OCTAVE campaign: Sources and distributions of formaldehyde on reunion Island, Atmosphere, 11, 140, https://doi.org/10.3390/atmos11020140, 2020.

Rocco, M., Baray, J.-L., Colomb, A., Borbon, A., Dominutti, P., Tulet, P., Amelynck, C., Schoon, N., Verreyken, B., Duflot, V., Gros, V., Sarda-Estève, R., Péris, G., Guadagno, C., and Leriche, M.: High resolution dynamical analysis of Volatile Organic Compounds (VOC) measurements during the BIO-MAÏDO field campaign (Réunion Island, Indian Ocean), J. Geophys. Res.-Atmos., 127, e2021JD035570, https://doi.org/10.1029/2021JD035570, 2022.

Rose, C., Chaumerliac, N., Deguillaume, L., Perroux, H., Mouchel-Vallon, C., Leriche, M., Patryl, L., and Armand, P.: Modeling the partitioning of organic chemical species in cloud phases with CLEPS (1.1), Atmos. Chem. Phys., 18, 2225–2242, https://doi.org/10.5194/acp-18-2225-2018, 2018.

Rose, C., Foucart, B., Picard, D., Colomb, A., Metzger, J.-M., Tulet, P., and Sellegri, K.: New particle formation in the volcanic eruption plume of the Piton de la Fournaise: specific features from a long-term dataset, Atmos. Chem. Phys., 19, 13243–13265, https://doi.org/10.5194/acp-19-13243-2019, 2019.

Samaké, A., Jaffrezo, J.-L., Favez, O., Weber, S., Jacob, V., Albinet, A., Riffault, V., Perdrix, E., Waked, A., Golly, B., Salameh, D., Chevrier, F., Oliveira, D. M., Bonnaire, N., Besombes, J.-L., Martins, J. M. F., Conil, S., Guillaud, G., Mesbah, B., Rocq, B., Robic, P.-Y., Hulin, A., Le Meur, S., Descheemaecker, M., Chretien, E., Marchand, N., and Uzu, G.: Polyols and glucose particulate species as tracers of primary biogenic organic aerosols at 28 French sites, Atmos. Chem. Phys., 19, 3357–3374, https://doi.org/10.5194/acp-19-3357-2019, 2019.

Shrivastava, M., Cappa, C. D., Fan, J., Goldstein, A. H., Guenther, A. B., Jimenez, J. L., Kuang, C., Laskin, A., Martin, S. T., Ng, N. L., Petaja, T., Pierce, J. R., Rasch, P. J., Roldin, P., Seinfeld, J. H., Shilling, J., Smith, J. N., Thornton, J. A., Volkamer, R., Wang, J., Worsnop, D. R., Zaveri, R. A., Zelenyuk, A., and Zhang, Q.: Recent advances in understanding secondary organic aerosol: Implications for global climate forcing, Rev. Geophys., 55, 509–559, https://doi.org/10.1002/2016RG000540, 2017.

Simoneit, B. R. T.: Biomass burning – a review of organic tracers for smoke from incomplete combustion, Appl. Geochem., 17, 129–162, https://doi.org/10.1016/S0883-2927(01)00061-0, 2002.

Simu, S. A., Miyazaki, Y., Tachibana, E., Finkenzeller, H., Brioude, J., Colomb, A., Magand, O., Verreyken, B., Evan, S., Volkamer, R., and Stavrakou, T.: Origin of water-soluble organic aerosols at the Maïdo high-altitude observatory, Réunion Island, in the tropical Indian Ocean, Atmos. Chem. Phys., 21, 17017–17029, https://doi.org/10.5194/acp-21-17017-2021, 2021.

Stahl, C., Crosbie, E., Bañaga, P. A., Betito, G., Braun, R. A., Cainglet, Z. M., Cambaliza, M. O., Cruz, M. T., Dado, J. M., Hilario, M. R. A., Leung, G. F., MacDonald, A. B., Magnaye, A. M., Reid, J., Robinson, C., Shook, M. A., Simpas, J. B., Visaga, S. M., Winstead, E., Ziemba, L., and Sorooshian, A.: Total organic carbon and the contribution from speciated organics in cloud water: airborne data analysis from the CAMP^{2}Ex field campaign, Atmos. Chem. Phys., 21, 14109–14129, https://doi.org/10.5194/acp-21-14109-2021, 2021.

Su, H., Cheng, Y., and Pöschl, U.: New Multiphase Chemical Processes Influencing Atmospheric Aerosols, Air Quality, and Climate in the Anthropocene, Accounts Chem Res., 53, 2034–2043, https://doi.org/10.1021/acs.accounts.0c00246, 2020.

Sun, W., Fu, Y., Zhang, G., Yang, Y., Jiang, F., Lian, X., Jiang, B., Liao, Y., Bi, X., Chen, D., Chen, J., Wang, X., Ou, J., Peng, P., and Sheng, G.: Measurement report: Molecular characteristics of cloud water in southern China and insights into aqueous-phase processes from Fourier transform ion cyclotron resonance mass spectrometry, Atmos. Chem. Phys., 21, 16631–16644, https://doi.org/10.5194/acp-21-16631-2021, 2021.

Triesch, N., van Pinxteren, M., Engel, A., and Herrmann, H.: Concerted measurements of free amino acids at the Cabo Verde islands: high enrichments in submicron sea spray aerosol particles and cloud droplets, Atmos. Chem. Phys., 21, 163–181, https://doi.org/10.5194/acp-21-163-2021, 2021.

Tsui, W. G., Woo, J. L., and McNeill, V. F.: Impact of aerosol-cloud cycling on aqueous secondary organic aerosol formation, Atmosphere, 10, 666, https://doi.org/10.3390/atmos10110666, 2019.

Vaïtilingom, M., Attard, E., Gaiani, N., Sancelme, M., Deguillaume, L., Flossmann, A. I., Amato, P., and Delort, A.-M.: Long-term features of cloud microbiology at the puy de Dôme (France), Atmos. Environ., 56, 88–100, https://doi.org/10.1016/j.atmosenv.2012.03.072, 2012.

Vaïtilingom, M., Deguillaume, L., Vinatier, V., and Delort, A.-M.: Potential impact of microbial activity on the oxidant capacity and organic carbon budget in clouds, P. Natl. Acad. Sci. USA, 110, 559–564, https://doi.org/10.1073/pnas.1205743110, 2013.

van Pinxteren, D., Plewka, A., Hofmann, D., Müller, K., Kramberger, H., Svrcina, B., Bächmann, K., Jaeschke, W., Mertes, S., Collett, J. L., and Herrmann, H.: Schmücke hill cap cloud and valley stations aerosol characterisation during FEBUKO (II): Organic compounds, Atmos. Environ., 39, 4305–4320, https://doi.org/10.1016/j.atmosenv.2005.02.014, 2005.

Verma, S. K., Kawamura, K., Chen, J., and Fu, P.: Thirteen years of observations on primary sugars and sugar alcohols over remote Chichijima Island in the western North Pacific, Atmos. Chem. Phys., 18, 81–101, https://doi.org/10.5194/acp-18-81-2018, 2018.

Verreyken, B., Brioude, J., and Evan, S.: Development of turbulent scheme in the FLEXPART-AROME v1.2.1 Lagrangian particle dispersion model, Geosci. Model Dev., 12, 4245–4259, https://doi.org/10.5194/gmd-12-4245-2019, 2019.

Verreyken, B., Amelynck, C., Brioude, J., Müller, J.-F., Schoon, N., Kumps, N., Colomb, A., Metzger, J.-M., Lee, C. F., Koenig, T. K., Volkamer, R., and Stavrakou, T.: Characterisation of African biomass burning plumes and impacts on the atmospheric composition over the south-west Indian Ocean, Atmos. Chem. Phys., 20, 14821–14845, https://doi.org/10.5194/acp-20-14821-2020, 2020.

Verreyken, B., Amelynck, C., Schoon, N., Müller, J.-F., Brioude, J., Kumps, N., Hermans, C., Metzger, J.-M., Colomb, A., and Stavrakou, T.: Measurement report: Source apportionment of volatile organic compounds at the remote high-altitude Maïdo observatory, Atmos. Chem. Phys., 21, 12965–12988, https://doi.org/10.5194/acp-21-12965-2021, 2021.

Wang, H., Kawamura, K., and Yamazaki, K.: Water-Soluble dicarboxylic acids, ketoacids and dicarbonyls in the atmospheric aerosols over the southern ocean and western pacific ocean, J. Atmos. Chem., 53, 43–61, https://doi.org/10.1007/s10874-006-1479-4, 2006.

Wang, M., Perroux, H., Fleuret, J., Bianco, A., Bouvier, L., Colomb, A., Borbon, A., and Deguillaume, L.: Anthropogenic and biogenic hydrophobic VOCss detected in clouds at the puy de Dôme station using Stir Bar Sorptive Extraction: Deviation from the Henry's law prediction, Atmos. Res., 237, 104844, https://doi.org/10.1016/j.atmosres.2020.104844, 2020.

Witkowski, B., Jain, P., and Gierczak, T.: Aqueous chemical bleaching of 4-nitrophenol brown carbon by hydroxyl radicals; products, mechanism, and light absorption, Atmos. Chem. Phys., 22, 5651–5663, https://doi.org/10.5194/acp-22-5651-2022, 2022.

World Health Organization – Regional Office for Europe: Review of evidence on health aspects of air pollution: REVIHAAP project: technical report, World Health Organization, Regional Office for Europe, https://apps.who.int/iris/handle/10665/341712 (last access: 21 March 2024), 2021.

Yao Liu, El Haddad, I., Scarfogliero, M., Nieto-Gligorovski, L., Temime-Roussel, B., Quivet, E., Marchand, N., Picquet-Varrault, B., and Monod, A.: In-cloud processes of methacrolein under simulated conditions – Part 1: Aqueous phase photooxidation, Atmos. Chem. Phys., 9, 5093–5105, https://doi.org/10.5194/acp-9-5093-2009, 2009.

Zhang, Q., Jimenez, J. L., Canagaratna, M. R., Allan, J. D., Coe, H., Ulbrich, I., Alfarra, M. R., Takami, A., Middlebrook, A. M., Sun, Y. L., Dzepina, K., Dunlea, E., Docherty, K., DeCarlo, P. F., Salcedo, D., Onasch, T., Jayne, J. T., Miyoshi, T., Shimono, A., Hatakeyama, S., Takegawa, N., Kondo, Y., Schneider, J., Drewnick, F., Borrmann, S., Weimer, S., Demerjian, K., Williams, P., Bower, K., Bahreini, R., Cottrell, L., Griffin, R. J., Rautiainen, J., Sun, J. Y., Zhang, Y. M., and Worsnop, D. R.: Ubiquity and dominance of oxygenated species in organic aerosols in anthropogenically-influenced Northern Hemisphere midlatitudes, Geophys. Res. Lett., 34, L13801, https://doi.org/10.1029/2007gl029979, 2007.

Zhang, T., Engling, G., Chan, C.-Y., Zhang, Y.-N., Zhang, Z.-S., Lin, M., Sang, X.-F., Li, Y. D., and Li, Y.-S.: Contribution of fungal spores to particulate matter in a tropical rainforest, Environ. Res. Lett., 5, 024010, https://doi.org/10.1088/1748-9326/5/2/024010, 2010.

Zhao, Y., Hallar, A. G., and Mazzoleni, L. R.: Atmospheric organic matter in clouds: exact masses and molecular formula identification using ultrahigh-resolution FT-ICR mass spectrometry, Atmos. Chem. Phys., 13, 12343–12362, https://doi.org/10.5194/acp-13-12343-2013, 2013.

Zhu, C., Kawamura, K., and Kunwar, B.: Organic tracers of primary biological aerosol particles at subtropical Okinawa Island in the western North Pacific Rim: organic biomarkers in the north pacific, J. Geophys. Res.-Atmos., 120, 5504–5523, 2015.